Hypoxia-Inducible Factor 1α Induces Fibrosis and Insulin Resistance in White Adipose Tissue

Nils Halberg, Tayeba Khan, Maria E. Trujillo, Ingrid Wernstedt-Asterholm, Alan D. Attie, Shariq Sherwani, Zhao V. Wang, Shira Landskroner-Eiger, Sean Dineen, Ulysses J. Magalang, Rolf A. Brekken and Philipp E. Scherer

Mol. Cell. Biol. **2009, 29(16):4467. DOI: 10.1128/MCB.00192-09.**
Published Ahead of Print 22 June 2009.

MOLECULAR AND CELLULAR BIOLOGY, Aug. 2009, p. 4467–4483 Vol. 29, No. 16
0270-7306/09/$08.00+0 doi:10.1128/MCB.00192-09

Hypoxia-Inducible Factor 1α Induces Fibrosis and Insulin Resistance in White Adipose Tissue▽§

Nils Halberg,[1,8] Tayeba Khan,[2] Maria E. Trujillo,[2,3] Ingrid Wernstedt-Asterholm,[1] Alan D. Attie,[4] Shariq Sherwani,[5] Zhao V. Wang,[1] Shira Landskroner-Eiger,[2] Sean Dineen,[6] Ulysses J. Magalang,[5] Rolf A. Brekken,[6] and Philipp E. Scherer[1,7]*

Touchstone Diabetes Center, Department of Internal Medicine,[1] Hamon Center for Therapeutic Oncology and Division of Surgical Oncology,[6] and Department of Cell Biology,[7] University of Texas Southwestern Medical Center, Dallas, Texas 75390; Department of Cell Biology, Diabetes Research Center, Albert Einstein Cancer Center, Albert Einstein College of Medicine, Bronx, New York 10461[2]; Lead Optimization Pharmacology, Merck Research Laboratories, Rahway, New Jersey 07065[3]; Department of Biochemistry, University of Wisconsin—Madison, Madison, Wisconsin 53706-1544[4]; Division of Pulmonary, Allergy, Critical Care and Sleep Medicine, The Ohio State University, Columbus, Ohio 43210[5]; and Department of Biomedical Sciences, Faculty of Health Science, University of Copenhagen, Copenhagen 2100, Denmark[8]

Received 10 February 2009/Returned for modification 19 March 2009/Accepted 5 June 2009

Adipose tissue can undergo rapid expansion during times of excess caloric intake. Like a rapidly expanding tumor mass, obese adipose tissue becomes hypoxic due to the inability of the vasculature to keep pace with tissue growth. Consequently, during the early stages of obesity, hypoxic conditions cause an increase in the level of hypoxia-inducible factor 1α (HIF1α) expression. Using a transgenic model of overexpression of a constitutively active form of HIF1α, we determined that HIF1α fails to induce the expected proangiogenic response. In contrast, we observed that HIF1α initiates adipose tissue fibrosis, with an associated increase in local inflammation. "Trichrome- and picrosirius red-positive streaks," enriched in fibrillar collagens, are a hallmark of adipose tissue suffering from the early stages of hypoxia-induced fibrosis. Lysyl oxidase (LOX) is a transcriptional target of HIF1α and acts by cross-linking collagen I and III to form the fibrillar collagen fibers. Inhibition of LOX activity by β-aminoproprionitrile treatment results in a significant improvement in several metabolic parameters and further reduces local adipose tissue inflammation. Collectively, our observations are consistent with a model in which adipose tissue hypoxia serves as an early upstream initiator for adipose tissue dysfunction by inducing a local state of fibrosis.

The dramatic rise in the prevalence of obesity has lead to increased efforts aimed at gaining a better understanding of the physiology and pathophysiology of adipose tissue and adipocytes. One of the more-surprising features of adipose tissue described over the past 10 years is the realization that adipose tissue in general and adipocytes in particular have the potential to be a rich source of a vast array of secretory proteins. Since infiltrating immune cells, most notably monocytes, are known to have a profound effect on adipocytes, interest in the stromal fraction of adipose tissue has increased considerably. These stromal components consist of fibroblastlike preadipocytes, endothelial cells, vascular smooth muscle cells, neurons, and immune cells. It is currently not established how these stromal components interact with adipocytes during adipose tissue expansion. The nature of the local endothelium, a key constituent of the vasculature, has received limited attention to date. Destruction of local endothelial cells results in a reduction in fat mass during times of excess caloric intake independent of food intake (2, 30, 38). Functioning through an as yet unidentified mechanism, such a reduction in fat mass results in decreased levels of steatosis in the liver and enhanced glucose tolerance. These metabolic improvements are somewhat surprising, considering that the forced reduction of fat mass in the context of lipodystrophies leads to a decrease rather than an increase in systemic insulin sensitivity (30, 36). These observations highlight the need for a better understanding of the adipose tissue vasculature.

During times of positive energy balance, adipose tissue absorbs the energy surplus by increasing both cell size and number. The ability of adipose tissue to expand critically depends on vascular outgrowth (4). At the same time, the increased adipocyte size requires oxygen to diffuse over longer distances prior to reaching adipocyte mitochondria; this is evident by a decreased partial oxygen pressure (20 mmHg versus 40 mmHg) in obese versus lean mice, respectively (20, 37, 53). Hypoxia in obese adipose tissue has been observed by several groups and results in the induction of the key hypoxia regulator, hypoxia-inducible factor 1 (HIF1) (20, 37, 49, 53). HIF1 is a heterodimer consisting of the oxygen-regulated HIF1α subunit and the constitutively expressed HIF1β (39). During normoxia, HIF1α is rapidly degraded by an oxygen-dependent

* Corresponding author. Mailing address: Touchstone Diabetes Center, Department of Internal Medicine, University of Texas Southwestern Medical Center, 5323 Harry Hines Blvd., Dallas, TX 75390-8549. Phone: (214) 648-8715. Fax: (214) 648-8720. E-mail: Philipp.Scherer@utsouthwestern.edu.

§ Supplemental material for this article may be found at http://mcb.asm.org/.

▽ Published ahead of print on 22 June 2009.

hydroxylation of two proline residues (P402/P564 in human HIF1α), which enables binding to an E3 ligase complex, thus targeting the protein for proteasomal degradation. Under hypoxic conditions, the level of prolyl hydroxylation is reduced, and as a consequence, the protein accumulates and translocates into the nucleus, where it binds to hypoxia response elements in concert with HIF1β and p300. The stability of HIF1α can be uncoupled from the local oxygen pressure by removal of the "oxygen degradation domain" (ΔODD; lacking amino acids 401 through 603) that comprises the two critical proline residues. As a result, the half-life of HIF1α increases from 5 min to approximately 60 min (23).

Here, our objectives were to address specifically the physiological consequences of the local hypoxia in adipose tissue and the concomitant upregulation of HIF1α. Taken together, we propose that HIF1α upregulation represents one of the earliest events during adipose tissue expansion and an important step in the sequential process of obesity-associated adipose tissue dysfunction.

MATERIALS AND METHODS

Materials. Phosphate-buffered saline (PBS) was obtained from EMD Biochemicals (Gibbstown, NJ), and 10% PBS-buffered formalin was purchased from Thermo Fischer Scientific (Waltham, MA). All other chemicals were obtained from Sigma-Aldrich.

Animals. The Institutional Animal Care and Use Committee of University of Texas Southwestern Medical Center, Dallas, the Albert Einstein College of Medicine, and The Ohio State University approved all animal experiments. HIF1α transgenic mice were generated by subcloning the human HIF1α gene containing a deletion between amino acids 401 and 603, which corresponds to the oxygen degradation domain (a kind gift from Frank Bunn, Brigham and Women's Hospital, Harvard University), into a plasmid containing the 5.4-kb aP2 promoter (kindly provided by Bruce Spiegelman, Dana Farber) and a conventional 3′ untranslated region (6). Following linearization, the construct was injected into FVB-derived blastocysts. Transgene-positive offspring were then genotyped using PCR with the following primer set: 5′CAAGAAGCCCTAACGTGTTTAT and 5′GTGATGTAGTAGCTGCATGA. HIF1α transgenic *ob*/*ob* mice were generated by mating heterozygous HIF1α transgenic mice with heterozygous leptin-deficient mice (*ob*/+) in a pure FVB background. Mouse mammary tumor virus-polyoma middle T antigen mice, originally generated by William Muller (16), were bred in-house. For the refined time course and hypoxia chamber studies, C57BL/6 wild-type mice were used.

Mice were maintained on a 12-h dark/12-h light cycle and housed in groups of two to four, with unlimited access to water, chow (no. 5058; LabDiet), or a high-fat diet (HFD) (no. D12492; Research Diets, Inc.), as indicated for the individual experiments. All experiments were conducted using littermate-controlled male mice. All HFD experiments were initiated at the age of 6 weeks.

Oral glucose tolerance test (OGTT). Mice were fasted for 2 h (starting at 10 a.m.) prior to administration of glucose (2.5 g/kg body weight) by gavaging. At the indicated time points, venous blood samples were collected in heparin-coated capillary tubes from the tail vein. Glucose was measured using an oxidase-peroxidase assay (Sigma-Aldrich). Mice did not have access to food throughout the experiment.

Insulin tolerance test. Mice were fasted for 6 h (starting at 10 a.m.) prior to administration of insulin (Novo Nordisk, Bagsvaerd, Denmark) at 1 mU/kg body weight by intraperitoneal (i.p.) injection. At the indicated time points, venous blood samples were collected in heparin-coated capillary tubes from the tail vein. Glucose was measured using an oxidase-peroxidase assay (Sigma-Aldrich). Mice were denied food throughout the experiment.

Hypoxia chamber. Male C57/B6 mice were acclimated to custom-made Plexiglas chambers with dimensions of 31 by 18.5 by 17 cm for 48 h prior to the start of continuous hypoxia (CH) or room air (RA) exposure. At the start of the experiment, the mice were placed in the custom-made sealed Plexiglas chambers and exposed to CH or RA. CH exposure was done by a gas control delivery system, using a hypoxic gas mixture (10% O_2, balance N_2). A decrease in the FiO_2 level to 10% was immediately achieved within 5 min by flushing the chamber with the hypoxic gas mixture at an appropriate high flow rate to lower the oxygen content in the cage. The flow rate was then lowered to 1 liter/min for the duration of the hypoxic exposure. The use of multiple inputs into the chamber was used to produce a uniform FiO_2 level throughout the cage. The O_2 concentration inside the chamber was continuously monitored using a gas analyzer (OxyStar-100; CWE, Inc., Ardmore, PA). A similar Plexiglas chamber was used for the animals exposed to the RA control group, except that they were exposed to RA.

The mice were kept at hypoxia for 48 h and 5 days, and all tissue harvesting was performed within 10 min after the mice were taken out of the chambers. Food was withdrawn for 4 h during the day of tissue harvesting. The animals were sacrificed using isoflurane.

In vivo insulin signaling. Mice were fasted for 6 h (starting at 10 a.m.) before an i.p. injection of 1.5 mU/kg body weight of insulin (Novo Nordisk, Bagsvaerd, Denmark). A total of 10 min after injection, the liver was excised and snap-frozen in liquid nitrogen.

Lipopolysaccharide challenge. Eight-week-old male mice were injected i.p. with 0.3 μg/g body weight of lipopolysaccharide (Sigma-Aldrich) at 8 a.m. At 5 p.m., subcutaneous and epididymal subcutaneous white adipose tissue were excised from the mice and stored in RNAlater (Ambion, Foster City, CA) until further processing.

BAPN treatment. A total of 100 μg/g body weight of β-aminoproprionitrile (BAPN) fumarate salt (Sigma-Aldrich) was administered daily by i.p. injection for the remaining 14 days of a 5-week HFD experiment.

PPARγ agonist treatment. The peroxisome proliferator-activated receptor γ (PPARγ) agonist 2-(2-[4-phenoxy-2-propylphenoxy]ethyl) indole-5-acetic acid (COOH) was a kind gift from Merck Research Laboratories (Rahway, NJ). COOH was administered to 8-week-old FVB mice through oral gavaging daily for 10 days (10 mg/kg body weight). Six hours after last being gavaged, the mice were sacrificed, and tissues were immediately frozen in liquid nitrogen.

Quantitative real-time PCR analysis. Mice were euthanized with isoflurane (Aerrane, Baxter, IL), and the appropriate tissues were excised and snap-frozen in liquid nitrogen. Total RNA were isolated following tissue homogenization in Trizol (Invitrogen, Carlsbad, CA) using a TissueLyser (Qiagen, Valencia, CA) and isolated using the RNeasy RNA extraction kit (Qiagen). The quality and quantity of the RNA were determined by absorbance at 260/280 nm. cDNA was prepared by reverse transcribing 1.5 μg RNA with SuperScript III reverse transcriptase (Invitrogen) and oligo$(dT)_{20}$ (Invitrogen). The following primer sets were used for quantitative reverse transcriptase PCR (RT-PCR): F4/80 (forward, 5′-CTTTGGCTATGGGCTTCCAGTC-3′; reverse, 5′-GCAAGGAGGACAGAGTTTATCGTG-3′), vascular endothelial growth factor A (VEGFa) (forward, 5′-GGAGATCCTTCGAGGAGCACTT; reverse, 5′-GGCGATTTAGCAGCAGATATAAGAA), CD31/PECAM-1 (forward, 5′-ATGACCCAGCAACATTCACA-3′; reverse, 5′-CGACAGGATGGAAATCAACAA), Flt-1 (forward, 5′-TGCCTACCTCACCTGTTTCC-3′; reverse, 5′-AAGGACCATCCCACTGTCTG-3′), Tie2 (forward, 5′-AAGCAACCCAGCCTTTTCTC-3′; reverse, 5′-TGAGCATTCTCCTTTGGAC-3′), glucose transporter 1 (GLUT1) (forward, 5′-CCTGTCTCTTCCTACCCAACC-3′; reverse, 5′-GCAGGAGTGTCCGTGTCTTC-3′), lysyl oxidase (LOX) (forward, 5′-CCACAGCATGGACGAATTCA-3′; reverse, AGCTTGCTTTGTGGCCTTCA-3′), Col1a1 (forward, 5′-GTGCTCCTGGTATTGCTGGT-3′; reverse, 5′-GGCTCCTCGTTTTCCTTCTT-3′), Col3a1 (forward, 5′-GGGTTTCCCTGGTCCTAAAg-3′; reverse, 5′-CCTGGTTTCCCATTTTCTCC-3′), Col6a1 (forward, 5′-GATGAGGGTGAAGTGGGAGA-3′; reverse, 5′-CAGCACGAAGAGGATGTCAA-3′), elastin (forward, 5′-TGGTATTGGTGGCATCGG-3′; reverse, 5′-CCTTGGCTTTGACTCCTGTG-3′), wild-type HIF1α (forward, 5′-CAAGATCTCGGCGAAGCAA; reverse, 5′-GGTGAGCCTCATAACAGAAGCTTT-3′), and hypoxanthine phosphoribosyltransferase (forward, 5′-AGCAGTACAGCCCCAAAA-3′; reverse, 5′-TTTGGCTTTTCCAGTTTCA-3′). For all quantitative RT-PCR experiments, the results were calculated using the threshold cycle method (32), using hypoxanthine phosphoribosyltransferase for normalization. The PCR product was quantified using the Sybr green method (Roche).

Gene expression profiling. For gene expression profiling experiments, total cRNA was synthesized from subcutaneous and epididymal white adipose tissue and spotted onto a mouse Illumina BeadArray (47K array) platform (Illumina, Inc., San Diego, CA). Change and significance were calculated based on three independent replicates. Gene lists and cluster analyses of the data sets were performed using Spotfire software (Tibco Software Inc., Sommerville, MA) and David Bioinformatics Resource (http://david.abcc.ncifcrf.gov/). For a comparison between 4-week-old and 10-week-old wild-type and *ob*/*ob* C57/B6 mice, we utilized the database generated and verified at the University of Wisconsin, Madison (27), available at http://diabetes.wisc.edu/index.php.

Blood vessel stains. To stain for functional blood vessels, mice were injected with 100 μg of biotinylated *Griffonia* (*Bandeiraea*) *simplicifolia* lectin (Vector Laboratories, Burlingame, CA) through the tail vein. Three minutes later, the

animal was perfusion fixed through the left ventricle with 1% paraformaldehyde, and the epididymal adipose tissue was excised for further fixation overnight in 10% PBS-buffered formalin. Tissues were then embedded in paraffin and cut in 5-μm sections. The lectin was visualized using a Cy3-labeled streptavidin (Vector Labs).

Adipocyte histology: H&E, Masson's trichrome, and picrosirius red. The relevant fat pads were excised and fixed in 10% PBS-buffered formalin for 24 h. Following paraffin embedding and sectioning (5 μm), the tissues were stained with hematoxylin and eosin (H&E), Masson's trichrome stain, and picrosirius red. To determine adipocyte size, pictures of the H&E staining were obtained using the Nikon Coolscope and analyzed using ImageJ software. Two hundred cells/sample were included in the analysis of six mice for each genotype. Images of Masson's trichrome staining were acquired with the Nikon Coolscope and used to quantify areas containing fibrillar collagens, as shown with blue staining (mainly collagen I and III) using the ImageJ software. The picrosirius red stains were visualized under polarized light and provide an additional way to visualize fibrillar collagen.

Hypoxyprobe staining. To allow for the assessment of the hypoxic regions, mice were injected i.p. with 60 mg/kg pimonidazole (Hypoxyprobe-1 plus kit; Chemicon International, Temecula, CA) 30 minutes prior to sacrifice. Tissues were excised, fixed in 10% normal formalin buffer, processed, and then paraffin embedded. Sections were stained according to the manufacturer's instructions. In particular, samples were incubated with monoclonal antibody 1 conjugated with fluorescein isothiocyanate at a 1:100 dilution for thirty minutes at room temperature. A secondary anti-fluorescein isothiocyanate monoclonal antibody was applied at a 1:100 dilution for 30 minutes. Staining was then visualized using DAB chromogen A. Sections were rinsed and counterstained with hematoxylin and then imaged using the Zeiss Axioskop plus with an AxioCam MRc camera, with either the 10× objective/0.3 numerical aperture or the 40× objective/0.65 numerical aperture.

Immunohistochemistry. Formalin-fixed, paraffin-embedded sections were stained for immunoreactive MAC-2 and HIF1α using rat anti-mouse MAC-2 (Cedarlane Laboratories, Ontario, Canada) and mouse anti-human HIF1α (Novus Biologicals, Littleton, CO). Binding of primary antibody was visualized using DAB chromogen A (Dako, Glostrup, Denmark). Counterstaining was performed with 70% hematoxylin. Images were acquired using the Nikon Coolscope. The HIF1α antibodies pick up an epitope in the ODD domain of HIF1α. This domain is missing in the HIF1α transgene.

Hydroxyproline content. A modified protocol of that described by Woessner (51) was utilized to determine the hydroxyproline content. In brief, 100 mg of frozen adipose tissue was heated in 6 N HCl at 110°C overnight in sealed tubes. Samples were then heated at 110°C for 48 h until they were dry. After 20 min of incubation with chloramine-T (Sigma-Aldrich) at room temperature, *p*-dimethylamino benzaldehyde (Fisher Scientific) was added for 15 min at 60°C. A standard curve was generated using *cis*-4-hydroxy-L-proline (Sigma-Aldrich), and the absorbance was read at 540 nm.

Isolation of peritoneal macrophages. To isolate mouse primary macrophages, 1 ml of 4% thioglycolate (Sigma-Aldrich) was injected i.p. Three days following the injection, peritoneal cells were harvested by lavaging (9). Cells were pelleted by centrifugation at 1,000 rpm and then resuspended in Dulbecco modified Eagle medium. After 6 h of incubation at 37°C, the adherent macrophages were washed three times in PBS and then harvested directly in Trizol (Invitrogen) for quantitative RT-PCR analysis.

Liver triglyceride. Liver triglycerides were measured, as described by Kim and coworkers (29). Briefly, total liver lipids were isolated by a 2:1 chloroform-methanol extraction. Triglycerides in the resulting lipid fraction were determined using the Infinity triglyceride assay (Thermo Fisher Scientific).

HIF1α transcription factor assay. HIF1α DNA binding was measured using the HIF1α EZ-TFA transcription factor assay (Millipore, Billerica, MA) according to the manufacturer's instructions. Briefly, snap-frozen tissue was lysed using the Dounce homogenizer in a hypotonic lysis buffer (10 mM HEPES [pH 7.9], 1.5 $MgCl_2$, 10 mM KCl, 0.5 mM dithiothreitol, 0.1% Triton X-100). Following a low spin and removal of the upper fat layer, nuclei were isolated by centrifugation at 3,000 rpm for 5 min at 4°C. Nuclear material was then extracted in 20 mM HEPES (pH 7.9), 350 mM NaCl, 1.5 mM $MgCl_2$, 0.2 mM EDTA (pH 8), 0.5 mM dithiothreitol, 25% glycerol, and protease inhibitors (Roche, Indianapolis, IN). Nuclear HIF1α was captured using a biotinylated probe containing the hypoxia response element and then visualized using a rabbit anti-HIF1α primary antibody. The resulting chemiluminescence was detected by the Polarstar Optima (BMG Labtech).

Immunoblotting. Frozen tissue was homogenized using the TissueLyser (Qiagen) in TNE buffer (50 mM Tris-HCl [pH 7.6], 150 mM NaCl, 5 mM EDTA, and phosphatase inhibitors [Sigma-Aldrich] and protease inhibitor [Roche]), followed by low spinning and removal of the fat cake. After addition of Triton X-100 to a final concentration of 1%, the protein concentration was determined using a bicinchoninic acid assay kit (Pierce). Proteins were separated on a 4 to 12% bis-Tris gel (Invitrogen) and transferred to a polyvinylidene difluoride membrane (Millipore). Rabbit anti-mouse LOX (a kind gift from Ian Hornstra, Washington University), goat anti-Akt (sc-1618; Santa Cruz Biotechnology), rabbit anti-p-Akt (sc-7985-R; Santa Cruz Biotechnology), and rabbit anti-mouse GDI (a kind gift from Perry Bickel, University of Texas Health Science Center, Houston) were used as primary antibodies. The primary antibodies were detected with secondary immunoglobulin Gs labeled with infrared dyes, emitting at 700 and 800 nm (Li-Cor Bioscience, Lincoln, NB) and visualized on the Li-Cor Odyssey infrared scanner (Li-Cor Bioscience). The scanned results were analyzed using Odyssey version 2.1 software (Li-Cor Bioscience).

Statistical analysis. All results are given as means ± standard errors of the means. All statistical analysis was performed using SigmaStat 2.03 software (Systat Software, Point Richmond, CA). Differences between the two groups over time (indicated in relevant figure legends) were determined by a two-way analysis of variance (ANOVA) for repeated measures, with a subsequent Tukey's post hoc test. For comparison of two independent groups, Student's *t* test was used. The level of significance in the cluster analysis was determined by the EASE software, with the modified Fischer *P* value (http://david.abcc.ncifcrf.gov/helps/functional_annotation.html#E4). Significance was accepted at a *P* value of <0.05.

RESULTS

Angiogenic capacity of white adipose tissue. As in any other soft tissue undergoing rapid growth, the angiogenic potential of white adipose tissue during fat expansion is extremely important and may in fact be rate limiting. Using conventional immunohistochemical methods for the detection of tissue hypoxia, we established that obese (*ob*/*ob*) but not lean (wild-type) adipose tissue suffers from hypoxia (Fig. 1A, top). Such observations are in line with observations reported by several other groups (20, 37, 53). To further ensure that the signal observed is specific, we examined a mammary fat pad in the mouse mammary tumor virus-polyoma middle T antigen breast cancer model. In these mice, adipocytes proximal to the tumor are highly hypoxic, whereas adipocytes more distal from the tumor masses within the same fat pad do not suffer from the same degree of hypoxia (Fig. 1A, bottom). To examine this phenomenon of hypoxia in greater detail, we performed expression profiling on a number of genes known to be involved in the response to local tissue hypoxia. One of the most critical master mediators of the hypoxic response is the transcriptional activator HIF1α. Consistent with the persistent hypoxia experienced in expanding adipose tissue, HIF1α mRNA levels are significantly elevated in a genetic model of obesity, the leptin-deficient *ob*/*ob* mouse. While even young *ob*/*ob* mice have elevated levels compared to those of wild-type mice, HIF1α levels increase even further with age (Fig. 1B). Under the same conditions, neither gastrocnemius muscle nor liver manifests any significant alterations in HIF1α expression levels (Fig. 1B). Since HIF1α is prominently regulated at the posttranslational level (40), we further quantified the degree of nuclear HIF1α protein accumulation in the adipose tissue of wild-type and *ob*/*ob* mice. Consistent with the observations seen at the mRNA level, HIF1α protein levels were significantly increased in the nuclei of adipose tissue derived from *ob*/*ob* mice (Fig. 1C). In the obese state, however, it is well established that several types of immune cells infiltrate adipose tissue depots. In order to specify what cell type upregulates HIF1α, we performed an immunohistochemical analysis of HIF1α of wild-type versus *ob*/*ob* mice. As shown in Fig. 1D, the overall stain-

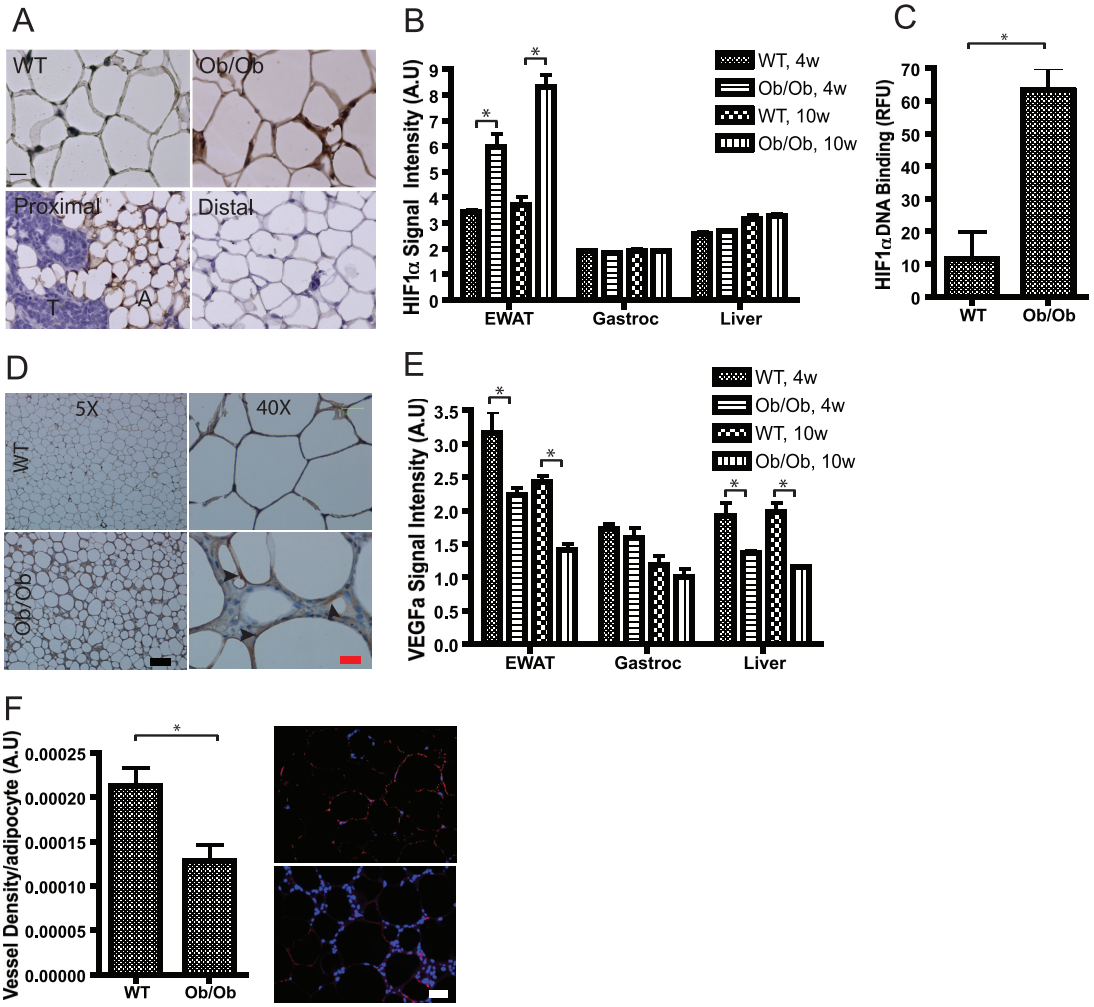

FIG. 1. Angiogenic capacity of white adipose tissue. (A) The top panels show hypoxia staining using the hypoxia probe pimonidazole in wild-type (WT) and *ob*/*ob* EWAT. The two bottom panels show the same hypoxia staining of adipocytes (A) located in close proximity to a mammary tumor (T) and another area of the same fat pad located more distal to the tumor. Bar corresponds to 20 μm. (B) Microarray expression analysis of HIF1α in the EWAT, gastrocnemius (Gastroc), and liver of 4-week-old (4w) and 10-week-old (10w) C57/B6 *ob*/*ob* and wild-type mice (five mice/group). A.U, arbitrary units. (C) Amount of HIF1α protein binding to the hypoxia response element in the nuclei from the EWAT of 8-week-old *ob*/*ob* and wild-type FVB mice (three mice/group). RFU, relative fluorescence units. (D) Immunohistochemical analysis of HIF1α in the EWAT of 8-week-old FVB wild-type and *ob*/*ob* mice. The two left panels show an overview of a fat pad, whereas the two right panels show closeup views of the same fat pads. Arrows denote staining close to lipid droplets but not in the inflamed area in between the adipocytes. The black bar represents 200 μm. The red bar represents 25 μm. (E) Microarray expression analysis of VEGFa in EWAT from 4- and 10-week-old C57/B6 *ob*/*ob* and wild-type mice in the EWAT, gastrocnemius, and liver (five mice/group). (F) Functional blood vessels in EWAT of 8-week-old *ob*/*ob* FVB and wild-type FVB mice visualized by tail vein injection of biotinylated lectin (*Griffonia simplicifolia*). Blood vessels are shown in red, and DAPI (4′,6-diamidino-2-phenylindole) staining of the nucleus is shown in blue. Quantification of vascular density was determined as percent Cy3 stain per field normalized to the number of adipocytes (three mice/group). Bar equals 50 μm. Panels B, C, E, and F were analyzed by Student's *t* test. ∗, $P < 0.05$.

ing increased markedly in the obese state. It is important to note, however, that the positive staining is within immediate proximity to the lipid droplet and not within interspersed immune cells. As predicted by mRNA analysis, the increased amount of immunoreactive HIF1α was not different between wild-type and *ob*/*ob* mice in the liver (see Fig. S1 in the supplemental material). While HIF1α protein is clearly stabilized and accumulates to a higher degree in the nuclear fraction of hypoxic adipose tissue, we examined whether this nuclear HIF1α effectively stimulates a proangiogenic program, similar to what many reports in the literature have described (1). To our surprise, we observed that the elevated levels of HIF1α failed to induce the expression of several of the established downstream targets of HIF1α, such as VEGFa (Fig. 1E). In contrast, mRNA levels for this highly angiogenic protein were significantly reduced in obese adipose tissue, while muscle and liver showed only limited alterations. In line with the decreased levels of VEGFa mRNA, a panel of additional factors with proangiogenic activity reveals that they are either unaffected or slightly reduced under the obesity-associated hypoxic conditions (see Fig. S2 in the supplemental material). To confirm the reduced vascular density in obese adipose tissue, we high-

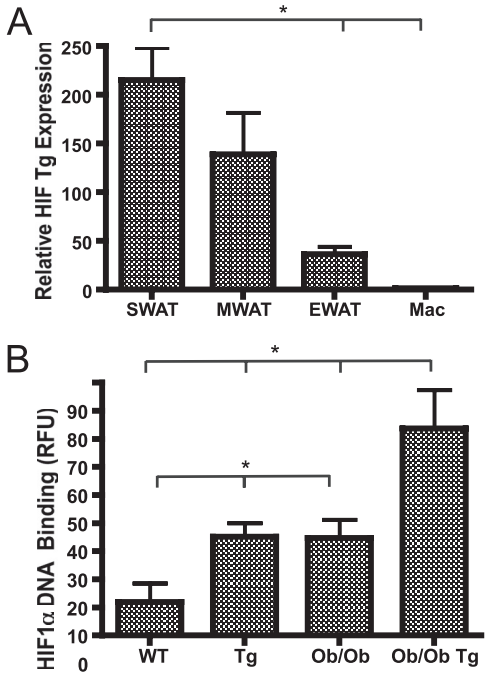

FIG. 2. Transgenic mouse overexpressing HIF1α in adipose tissue. (A) Quantitative RT-PCR analysis of the aP2 promoter-driven expression of HIF1α-ΔODD shows that the transgene (Tg) expression is very limited in isolated primary macrophages. Within the different fat pads, the transgene expression is heterogeneous, with highest expression in SWAT and lowest in EWAT. (B) Compared to wild-type and *ob*/*ob* littermates, the transgene expression results in a significant increase in overall SWAT HIF1α protein binding to the hypoxia response element in HIF1α-ΔODD and HIF1α-ΔODD-*ob*/*ob* (two mice/group). RFU, relative fluorescence units. Panels A and B were analyzed by Student's *t* test. *, $P < 0.05$.

lighted the vasculature of wild-type and *ob*/*ob* adipose tissue by injecting a labeled lectin to visualize functional blood vessels. As suggested by the decreased VEGFa expression, the vascular density in the obese adipose tissue was significantly reduced (Fig. 1F). This suggests that the obesity-associated increased levels of HIF1α are insufficient to enhance local angiogenesis. To further investigate the role of HIF1α in adipose tissue, we generated a transgenic mouse model in which the adipocyte-specific aP2 promoter drives the expression of a dominant-active form of human HIF1α.

Transgenic mouse overexpressing HIF1α in adipose tissue. The transgenic mice were engineered to express a dominant-active form of human HIF1α with a ΔODD under the control of the aP2 promoter. The aP2 promoter has been widely used to drive transgene expression in adipocytes and, depending on the integration site, also in macrophages. In this particular case, the mRNA of the transgenic ΔODD-HIF1α is expressed exclusively in adipocytes and only at very low levels in isolated primary macrophages (Fig. 2A; see also Fig. S3 in the supplemental material). Depending on the integration site of the transgene, the relative expression level of the transgenic cassette can also differ among different fat pads. We therefore compared the expression levels in three different white fat pads: epididymal white adipose tissue (EWAT), subcutaneous white adipose tissue (SWAT), and mesenteric white adipose tissue. We observed rather dramatic differences in the transgene expression levels among these three fat pads. The highest expression was observed in the SWAT and the lowest in the EWAT (Fig. 2A). Not only does this allow us to compare the metabolic phenotypes of wild-type and transgenic animals, but it also allows us to determine the impact of the transgene locally within different fat pads in the same mouse. We confirmed that transgene-mediated increases in HIF1α lead to higher functional levels of nuclear HIF1α protein, as judged by increased HIF1α DNA binding in the nuclei of SWAT in the transgenic animals (Fig. 2B). Importantly, we aimed to work within a physiological range of HIF1α overexpression. As apparent in Fig. 2B, we achieve DNA binding activity levels in transgenic wild-type mice that are comparable to levels observed in *ob*/*ob* mice, whereas the levels in transgenic *ob*/*ob* mice are about twofold above the baseline activity seen in *ob*/*ob* mice. While all transgenic approaches have the inherent disadvantage of creating a somewhat artificial environment, we believe that the overexpression within this narrow physiological range allows us to draw conclusions with respect to the direct metabolic impact of HIF1α in the context of obesity. Furthermore, it should be noted that by removing the ODD from the HIF1α cDNA, we also remove the N-terminal activation domain of HIF1α. The N-terminal activation domain has been implicated to be important for the differential effects seen between HIF1α and HIF2α (22).

Metabolic impact of HIF1α-ΔODD in white adipose tissue. On a normal chow diet as well as on an HFD, hemizygote transgenic mice display increased body weights (Fig. 3A and B). These differences in body weight were no longer apparent when we challenged the mice genetically with an *ob*/*ob* mutation (Fig. 3C). This is a much more extreme challenge than a simple HFD regimen, although from our previous results, we know that adipose tissue can be further expanded even in the *ob*/*ob* background via local overexpression of adiponectin (29). Interestingly, the HFD-induced increase in body weight paralleled a transgene dosage-dependent difference in adipocyte cell size (Fig. 3D). Adipocyte cell sizes were comparable between the transgenic and wild-type mice in the EWAT, whereas a marked difference was observed in the SWAT that expresses higher levels of transgenic HIF1α (Fig. 3D). Despite differences in average adipocyte size, local leptin production in the SWAT was not different (see Fig. S4 in the supplemental material).

We were hoping that the HIF1α overexpression would enable SWAT to act as a "metabolic sink," accommodating excess triglycerides in a fashion similar to that in our previously described model of adiponectin overexpression (29). To test whether this indeed resulted in improvements in the overall metabolic phenotype, we challenged the mice metabolically. Surprisingly, HIF1α hemizygote transgenic mice fed a chow diet or an HFD (for 12 weeks) both demonstrated decreased glucose tolerance during an OGTT, without differences in the glucose-induced insulin release compared to that of wild-type mice (Fig. 3E and F). Homozygote transgenic mice fed an HFD for only 5 weeks confirmed the results from the hemizygote transgenic mice and had increased body weight as well as increased glucose excursions during the OGTT (see Fig. S5 and S6 in the supplemental material). To determine whether the decreased glucose tolerance was an indirect consequence

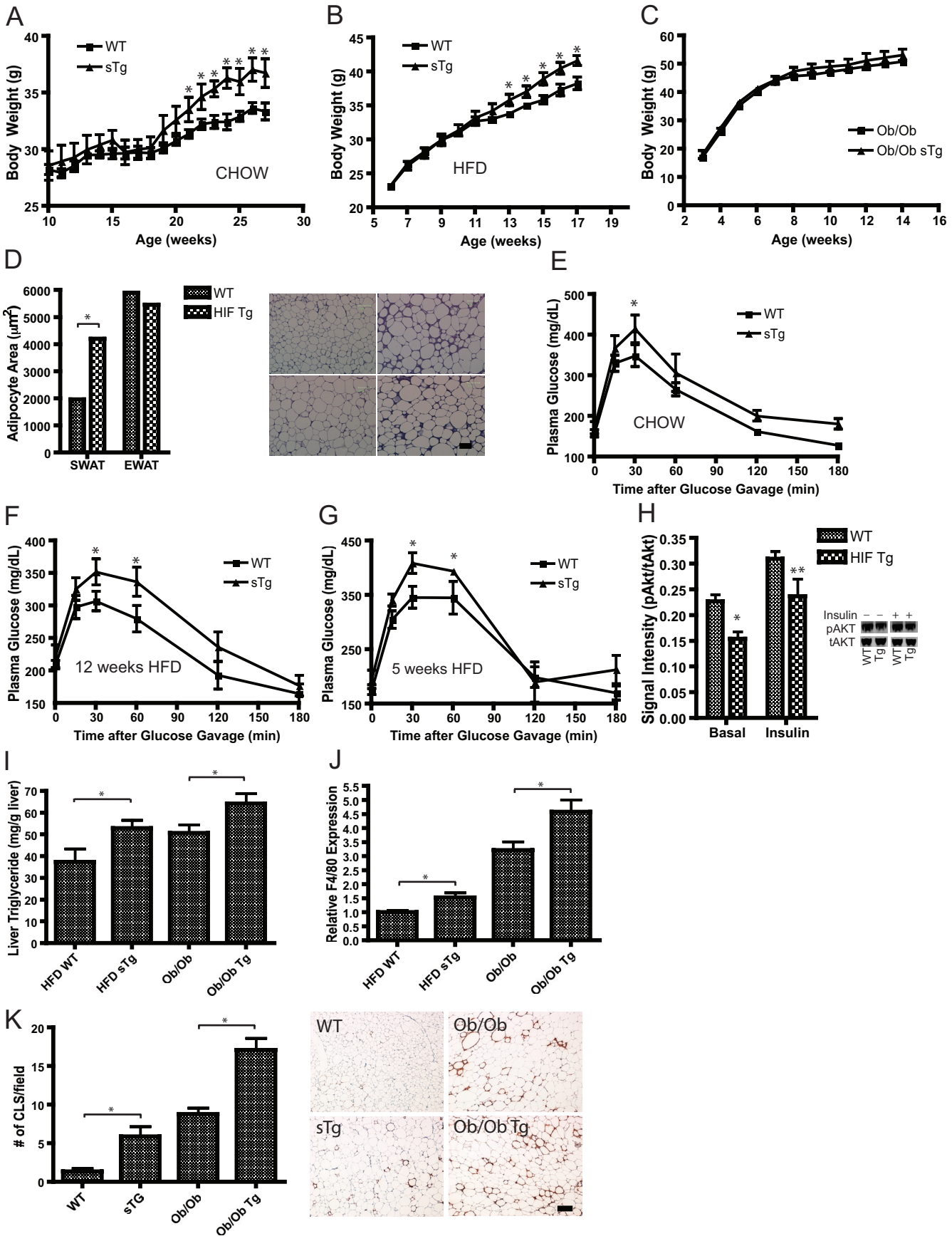

of the increased obesity or a direct effect of the transgene per se, we also performed an OGTT with mice fed an HFD for only 5 weeks as opposed to the experimental cohort shown above, in which the mice were kept on the diet for 12 weeks. At 5 weeks, the transgenic and wild-type animals did not yet differ in body weight. However, despite comparable adiposity, we still found a decreased glucose tolerance in the transgenic mice (Fig. 3G). This demonstrates a direct, adiposity-independent impact of the transgene on the glucose tolerance. In line with the decreased glucose tolerance during the OGTT, the transgenic mice had decreased liver insulin signaling, as detected by a decreased phospho-Akt-to-total Akt ratio, both in the basal and in the insulin stimulated state (Fig. 3H). This did not, however, amount to significant differences in the insulin tolerance test (see Fig. S7 in the supplemental material). In both the HFD-fed and the *ob*/*ob* transgenic animals, the decreased glucose tolerance was accompanied by additional signs of adipose tissue dysfunction, including increased liver triglycerides (Fig. 3I) and increased adipose tissue infiltration of macrophages, as judged by increased levels of F4/80 expression (Fig. 3J) and the frequency of crown-like structures (44) (Fig. 3K). The effects related to macrophage infiltration were again dose dependent on local transgene expression, since the increased F4/80 expression was seen only in the SWAT but not in EWAT (data not shown). With EWAT affected only marginally by the transgene, other systemic readouts such as fasting plasma levels of glucose, triglyceride, cholesterol, free fatty acids, glycerol, and lactate were not affected by the HIF transgene (see Table S1 in the supplemental material). This suggests that chronic exposure to HIF1α in fact causes a deterioration of glucose homeostasis.

Impact of HIF1α-ΔODD on gene transcription. Previous in vivo results employing a similar HIF1α dominant-active construct under the control of the keratin-14 promoter lead to an increase of 8- to 13-fold in VEGF expression (10). As might be expected from our initial finding in the *ob*/*ob* mouse, we did not detect any significant change in the SWAT VEGFa expression with the single transgene dose after 12 weeks of an HFD and in the HIF1α-ΔODD-*ob*/*ob* (see Fig. S8 and S9 in the supplemental material). We did not see a change with the double transgene dose after 5 weeks of an HFD (see Fig. S10 in the supplemental material) nor did this translate to significant changes in vascular marker gene expression, such as CD31, KDR, and Tie2, as measured by quantitative RT-PCR (see Fig. S8 to S10 in the supplemental material). Furthermore, HIF1α is known to induce nonaerobic glucose metabolism through induction of GLUT1, lactate dehydrogenase, and hexokinase (41). We probed for GLUT1 levels and determined that GLUT1 expression was not significantly affected by the transgene (data not shown). Similarly, we did not detect any significant alterations in the end product of anaerobic glycolysis, lactate, within SWAT (see Fig. S11 in the supplemental material) or in the respiratory exchange ratio, as measured in metabolic cage studies with the mice (data not shown).

TABLE 1. Gene cluster upregulation by HIF1α

Cluster	No. of genes	*P* value
Extracellular matrix	51	4.6×10^{-30}
Chemotaxis/inflammation	13	1.5×10^{-15}
Vasculature	19	3.1×10^{-3}
Sarcomere	11	1.2×10^{-2}

The lack of any angiogenic as well as glycolytic phenotypes prompted us to utilize a more global approach for the analysis of these fat pads. We performed gene expression profiling of SWAT and EWAT after 12 weeks of an HFD in wild-type and HIF1α-ΔODD transgenic mice to see if we could identify a specific set of genes influenced by HIF1α that has the potential to explain the negative metabolic consequences described above. The HIF1α overexpression in SWAT led to 557 upregulated genes (>1.5-fold) and 760 downregulated genes. As seen in many of the other assays, changes in EWAT were far less dramatic (data not shown). A functional cluster analysis (Table 1) highlights the major categories of induced genes. Remarkably, many of these genes are extracellular matrix components. In contrast, many genes whose expression was repressed are involved in T-cell mediated immune responses (Table 2). Consistent with the histological assessment, adipose tissue from transgenic mice is significantly more inflamed; several macrophage markers such as F4/80, CD68, and CSF1R, as well as monocyte chemoattractants (CCL2, CCL7, and CCL8), were induced. Table 3 highlights the data from the clustered gene pools. These data demonstrate a general upregulation of many extracellular matrix proteins, such as collagens col1α1, col3α1, col4α1, col6α1, col18α1, elastin, and lumican. There are also a number of noteworthy "classical" HIF1α targets on this list, including LOX, tissue inhibitor of metalloproteinase 1 (TIMP1), and connective tissue growth factor (CTGF) (11, 17, 18, 34). All of the changes listed are significantly altered in SWAT, with no significant changes in the EWAT expression levels for most of them, thus further highlighting the critical

FIG. 3. Metabolic impact of HIF1α-ΔODD in adipose tissue. Hemizygote transgenic mice (sTg) fed either chow (A) or an HFD (B) have elevated body weight compared to those of their littermates (six mice/group for the chow; nine mice/group for the HFD). WT, wild-type mice. (C) Transgene expression in the *ob*/*ob* background does not trigger a further increase in body weight (four mice/group). (D) Quantification of adipocyte size in the H&E staining of adipocytes in wild-type and HIF1α transgenic mice (Tg) after 12 weeks of an HFD. Bar = 100 μm. Five mice/group. (E to G) Circulating glucose levels measured during an OGTT in wild-type and hemizygote HIF1α-ΔODD mice (sTg) fed a chow diet (six mice/group) (E) and in mice fed an HFD for 12 weeks (F) and 5 weeks (G) (seven mice/group). (H) Basal- and insulin-stimulated (1.5 U/kg) changes in the ratio of phosphorylated (Ser473) Akt to total levels of Akt in the livers of wild-type and transgenic mice fed an HFD for 12 weeks. Hallmarks of dysfunctional fat are liver triglyceride accumulation (I), increased levels of F4/80 expression in SWAT, measured by quantitative RT-PCR (J), and increased frequency of crown-like structures (K). The increase in crown-like structures can be observed in HIF1α transgenic mice both fed an HFD for 12 weeks or crossed into the *ob*/*ob* background. The immunohistochemical analysis (J) shows the macrophage-specific protein MAC-2 in SWAT. Bar = 200 μm. Seven mice/group for the HFD group; six mice/group for mice in the *ob*/*ob* background. Panels A, B, C, E, F, and G were analyzed by a two-way ANOVA for repeated measurements; panels D, H, I, J, and K were analyzed by Student's *t* test. *, $P < 0.05$; **, $P = 0.07$.

TABLE 2. Gene clusters downregulated by HIF1α

Cluster	No. of genes	*P* value
T-cell immune response	99	1.9×10^{-32}
T-cell activation	28	4.0×10^{-20}
Humoral response	11	9.4×10^{-5}
Lymph node	9	2.6×10^{-4}

dependence on the levels of transgene expression. It is noteworthy that in contrast to the ECM proteins that are expressed at high levels and for which we see significant differences, the differences in the T-cell cluster genes were all based on differences of very low levels of expression. In addition, when we looked at these particular genes in the context of obesity, no major T-cell phenotype could be found (see Fig. S12 in the supplemental material).

Fibrosis in dysfunctional white adipose tissue. We wondered if these alterations in extracellular matrix constituents have any significant impact on general adipose tissue physiology. We recently described a systematic analysis of dysfunctional adipose tissue, with particular focus on the degree of extracellular matrix accumulation. We observed that obesity is associated with an overall increase in expression of several collagens and therefore proposed that obesity leads to a fibrotic state. A genetic disruption leading to a lack of local collagen VI accumulation results in an improved metabolic phenotype and a decrease in the local inflammatory state (28). Trichrome staining of adipose tissue specifically highlights the fibrillar collagens I and III, yielding a blue stain. Whereas trichrome staining of wild-type adipose tissue reveals very thin collagen sheets surrounding each adipocyte, adipose tissue from *ob*/*ob* mice contains very pronounced trichrome-positive "streaks" interspersed among the adipocytes (Fig. 4A). Notably, these trichrome-positive streaks are distinct from the previously described "crown-like structures" that are characteristic of necrotic adipocytes surrounded by macrophages (44). The trichrome-positive streaks often appear outside the crown-like structures and, therefore, define a distinct histologic entity in the tissue. Picrosirius red stains collagen I in orange and collagen III in green when visualized under polarized light.

TABLE 3. Overview of differentially expressed genes identified by the microarray cluster analysis

Gene	Gene definition	GenBank accession no.	EWAT results		SWAT results	
			Fold change in expression level	*P* value of <0.05?	Fold change in expression level	*P* value of <0.05?
Col1a1	Procollagen, type I, alpha 1	NM_007742.2	1.18	No	1.65	Yes
Col3a1	Procollagen, type III, alpha 1	NM_009930.1	−1.06	No	1.76	Yes
Col4a1	Procollagen, type IV, alpha 1	NM_009931.1	1.07	No	1.49	Yes
Col5a3	Procollagen, type V, alpha 3	NM_016919.1	−1.04	No	1.55	Yes
Col6a2	Procollagen, type VI, alpha 2	NM_146007.1	−1.25	No	1.84	Yes
Col18a1	Procollagen, type XVIII, alpha 1	NM_009929.2	−1.02	No	1.66	Yes
Eln	Elastin	NM_007925.2	−1.03	No	1.33	Yes
Lum	Lumican	NM_008524	1.06	No	1.73	Yes
Lox	Lysyl oxidase	NM_010728.1	1.39	Yes	1.44	Yes
Fn1	Fibronectin 1	XM_129845.3	1.15	No	1.56	Yes
Ctgf	Connective tissue growth factor	NM_010217	0.89	No	1.38	Yes
Mmp2	Matrix metalloproteinase 2	NM_008610.1	1.16	No	1.58	Yes
S100a4	S100 calcium binding protein	NM_011311.1	1.10	No	1.28	Yes
Vim	Vimentin	NM_011701.3	1.03	No	1.41	Yes
Timp1	Tissue inhibitor of metalloproteinase 1	NM_011593	2.29	No	2.44	Yes
Tie1	Tyrosine kinase receptor 1	NM_011587.1	−1.05	No	1.53	Yes
Tek	Endothelial-specific receptor tyrosine kinase	NM_013690.1	−1.09	No	1.46	Yes
Agpt2	Angiopoietin 2	NM_007426.2	1.00	No	1.85	Yes
Hp	Haptoglobin	NM_017370.1	−1.30	No	2.10	Yes
Lcn2	Lipocalin 2	NM_008491.1	1.63	No	4.15	Yes
Ccl2	C-C motif ligand 2	NM_011333.1	1.12	No	1.66	Yes
Ccl3	C-C motif ligand 3	NM_011337.1	1.96	No	1.71	Yes
Tlr13	Toll-like receptor 13	NM_205820.1	1.18	No	2.05	Yes
Cd68	CD68 antigen	NM_009853.1	1.06	No	2.41	Yes
Emr1	Epidermal growth factor-like module containing mucin-like, hormone receptor-like sequence 1	NM_010130.1	1.01	No	1.53	Yes
Atp6v0a1	ATPase, H^+ transporting, lysosomal V0 subunit isoform 1	NM_016920.1	−1.29	No	1.71	Yes
Atp6ap2	ATPase, H^+ transporting, lysosomal accessory protein 2	NM_027439	−1.05	No	1.55	Yes
Cd4	CD4 antigen	NM_013488.1	1.01	No	−1.71	Yes
Cd3e	CD3 antigen, epsilon polypeptide	NM_007648	−1.04	No	−26.07	Yes
Cd3g	CD3 antigen, gamma polypeptide	NM_009850.1	1.08	No	−21.97	Yes
Cd2	CD2 antigen	NM_013486.1	1.00	No	−5.90	Yes
Cd5	CD5 antigen	NM_007650.2	1.04	No	−8.87	Yes
Xcl1	Chemokine (C motif) ligand 1	NM_008510.1	−1.04	No	−2.45	Yes
Ccl5	Chemokine (C-C motif) ligand 5	NM_013653.1	−1.02	No	−11.76	Yes
Ccl21a	Chemokine (C-C motif) ligand 21a (leucine)	NM_011335.1	−2.09	No	−9.61	Yes
Ccl21c	Chemokine (C-C motif) ligand 21c (leucine)	NM_023052	−1.85	No	−9.64	Yes
Ccl21b	Chemokine (C-C motif) ligand 21b (serine)	NM_011124.3	−2.20	No	−9.98	Yes

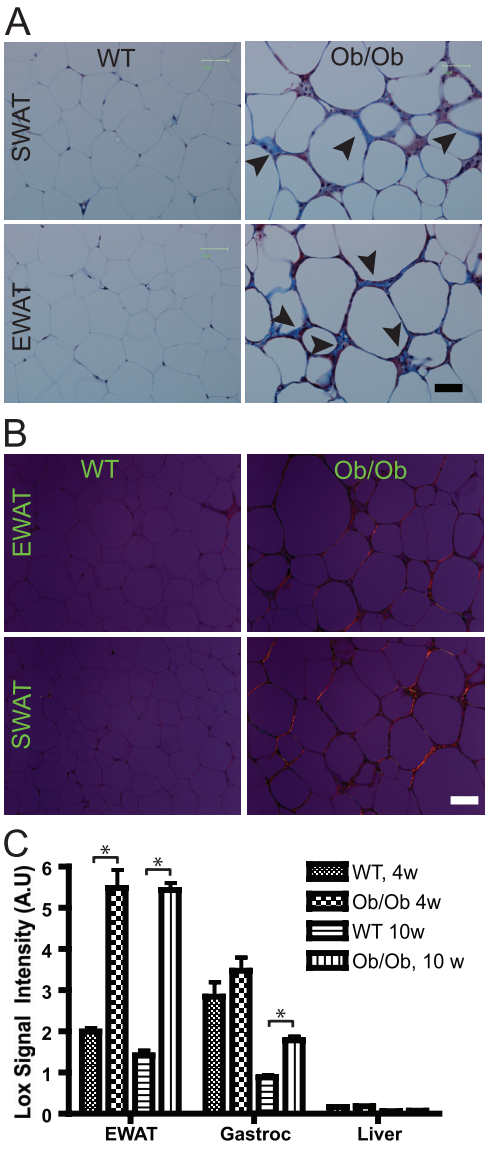

FIG. 4. Fibrosis in dysfunctional white adipose tissue. (A) Masson's trichrome staining of SWAT and EWAT from 8-week-old wild-type mice (WT) and *ob*/*ob* FVB mice. Fibrillar collagens, primarily collagen I and III, are stained with blue, as indicated with arrowheads. Nuclei are stained with deep purple, whereas keratin stains red. Bar corresponds to 50 μm; three mice/group. (B) Picrosirius red staining of SWAT and EWAT from 8-week-old wild-type and *ob*/*ob* FVB mice. Picrosirius red was visualized under polarized light and shows collagen I in orange and collagen 3 in green. (C) LOX expression in the EWAT, gastrocnemius (Gastroc), and liver for wild-type and 10-week-old (10w) *ob*/*ob* C57/B6 mice, measured by the microarray analysis (five mice/group). Panel C was analyzed by Student's *t* test. *, $P < 0.05$; 4w, 4 week old; A.U, arbitrary units.

Figure 4B confirms the existence of pronounced fibrotic streaks running through obese adipose tissue. It furthermore shows that the main collagen in adipose tissue is collagen I, as shown previously by Napolitano (33). Collagen deposition in the extracellular matrix reflects both changes in secretion of the particular collagen as well as the activity of extracellular matrix modulating proteins. In 10-week-old mice, the increased trichrome staining in the *ob*/*ob* mice is indeed partly a result of an increased level of expression of collagen III but not collagen I (see Fig. S13 and S14 in the supplemental material). As described previously, collagen VI follows the same pattern (see Fig. S15 in the supplemental material). More important than the collagens, we found an increased level of LOX in the EWAT of *ob*/*ob* mice compared to that of wild-type mice (Fig. 4C). LOX facilitates cross-linking and stabilization of collagens and elastins in the extracellular space and, thereby, increases insoluble matrix deposition and tensile strength (25). LOX is secreted as a 50-kDa proprotein and is cleaved by bone morphogenic protein 1 to produce the active 30-kDa protein. Like the observations for HIF1α (shown in Fig. 1B), the upregulation of LOX in obesity is restricted to adipose tissue. To further investigate the role of LOX, we first analyzed LOX expression during several treatments with an impact on metabolism. Treatment with a potently antidiabetic PPARγ agonist leads to a significant downregulation of LOX (see Fig. S16 in the supplemental material), suggesting that either a transcriptional repression of LOX or an inhibitor of the enzymatic activity associated with LOX may cause metabolic improvements, provided LOX is indeed causally linked to metabolic dysfunction. Whereas PPARγ agonist exposure leads to an improvement of the metabolic phenotype and a repression of LOX expression, treatment with bacterial lipopolysaccharide results in increased LOX expression (see Fig. S17 in the supplemental material). 3T3-L1 cells serve as a model for the differentiation of fibroblast-like preadipocytes to mature lipid-laden adipocytes. As has been reported for fibronectin, LOX is significantly downregulated (by approximately fivefold) during adipocyte differentiation (see Fig. S18 in the supplemental material). Thus, LOX is highly regulated in adipose tissue and follows a pattern of high expression under conditions of metabolic dysfunction.

HIF1α-mediated increase in fibrosis in adipose tissue. Having established that obese dysfunctional fat is associated with a generalized increase in extracellular matrix constituents and the primary cross-linking enzyme LOX, we considered whether the metabolic dysfunction observed in transgenic HIF1α-ΔODD mice could be explained by effects on several extracellular matrix constituents that we saw upregulated by microarray analysis. Indeed, both in the HFD-exposed HIF1α-ΔODD transgenic animals as well as in HIF1α-ΔODD transgenic animals in the *ob*/*ob* background, the levels of many extracellular matrix constituents are elevated relative to controls, as judged by quantitative RT-PCR (Fig. 5A; see also Fig. S19 in the supplemental material). Such extracellular matrix constituents include but are not limited to collagen I, III, and VI and elastin. Hydroxylation of proline residues is a characteristic posttranslational modification of collagens. Hydroxyproline content is therefore an efficient indicator of the overall collagen content of a tissue; as expected, the hydroxyproline content of adipose tissue is upregulated in a transgene dose-dependent manner (Fig. 5B).

In light of its pivotal role in establishing the extracellular matrix network in other tissues, LOX may also exert a similar role in the development of adipose tissue fibrosis. This is an enzyme that has not yet been studied in the context of adipose tissue. We observed transgene dose-dependent increases in LOX levels in the homo- and hemizygote HIF1α-ΔODD transgenic mice as well as an increased LOX expression in HIF1α-

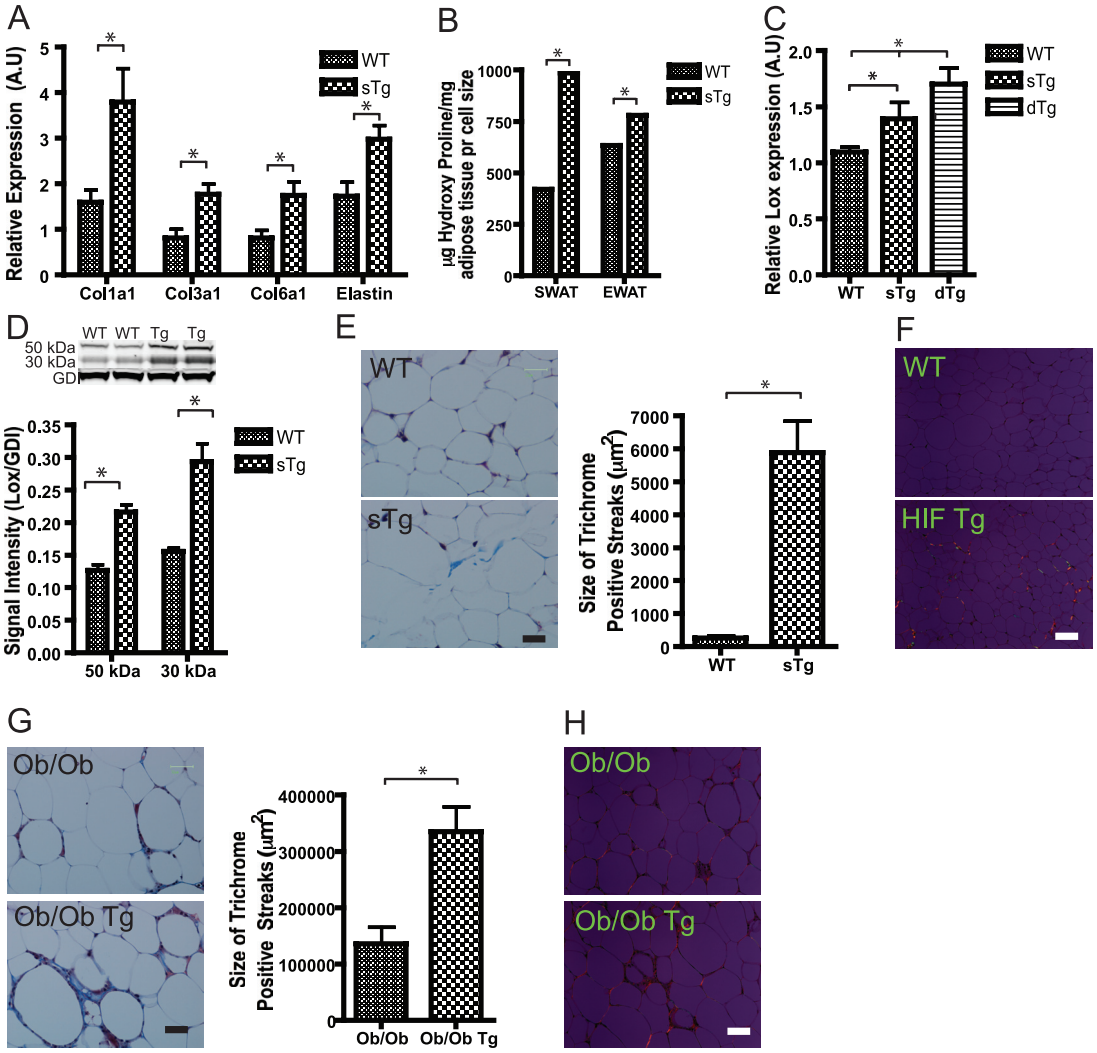

FIG. 5. HIF1α-mediated increased fibrosis in adipose tissue. (A) Col1a1, Col3a1, Col6a1, and elastin expression in SWAT from HIF1α-ΔODD mice and wild types (WT) fed an HFD for 12 weeks, as measured by quantitative RT-PCR (five mice/group). sTg, hemizygote transgenic mice; A.U, arbitrary units. (B) Hydroxyproline content in SWAT and EWAT of HIF1α-ΔODD and wild-type littermates fed an HFD for 12 weeks. Values are normalized to the size of the extracellular matrix space per field (six mice/group). (C) SWAT content of LOX mRNA levels in wild-type, hemizygote, and homozygote transgenic mice (dTg) after 5 weeks of an HFD, as measured by quantitative RT-PCR (five mice/group). (D) Protein levels of both the 50-kDa prepeptide and the 30-kDa active form of LOX in the SWAT of HIF1α-ΔODD and wild-type littermates fed an HFD for 12 weeks, as measured by Western blot analysis. Results were normalized to those of GDI (four mice/group). Tg, transgenic mice. (E) Quantification of the size of the trichrome-laden streaks through the adipose tissue in the SWAT from HIF1α-ΔODD mice versus wild types after 5 weeks of an HFD. Trichrome staining stains collagen fibers in blue, keratin in red, and nuclei in purple. The blue collagen fibers were quantified by measuring the blue area using ImageJ. Bar corresponds to 25 μm. (F) Picrosirius red staining of SWAT from HIF1α-ΔODD mice versus wild types after 5 weeks of an HFD, showing collagen I in orange and collagen III in green. Bar corresponds to 50 μm. (G) Quantification of the trichrome-stained streaks of SWAT of 18-week-old *ob*/*ob* and HIF1α-ΔODD-*ob*/*ob* mice. Bar corresponds to 25 μm. (H) Picrosirius red staining of SWAT from 18-week-old HIF1α-ΔODD and HIF1α-ΔODD-*ob*/*ob* mice. Bar corresponds to 50 μm. Five mice/group for the HFD group and four mice/group for the *ob*/*ob* group. Panels A, B, C, D, E, and G were analyzed by Student's *t* test. ∗, $P < 0.05$.

ΔODD-*ob*/*ob* mice compared to that of *ob*/*ob* mice (Fig. 5C; see also Fig. S20 in the supplemental material). This upregulation at the mRNA level translates into a significant elevation of LOX at both the levels of the 50-kDa propeptide and the active 30-kDa protein (Fig. 5D). In fact, LOX expression is already significantly increased after only 5 weeks of HFD, before we could detect any differences in F4/80 or collagen I or III expression (data not shown). Additionally, at this early time point, we were unable to detect any trichrome or picrosirius red laden streaks in SWAT of the wild-type animals, whereas they were present in the transgenic animals (Fig. 5E and F). As expected, such effects were absent in EWAT displaying low transgene levels (data not shown). The enhanced collagen accumulation became more apparent as the obese phenotype becomes more severe. In particular, the HIF1α-ΔODD-*ob*/*ob* expression in SWAT increased the trichrome- and picrosirius red-stained regions further, resulting in a doubling of the already heavily collagen-laden obese fat (Fig. 5G and H).

Inhibition of LOX by BAPN treatment leads to an improved metabolic phenotype. Given that LOX is a well-established

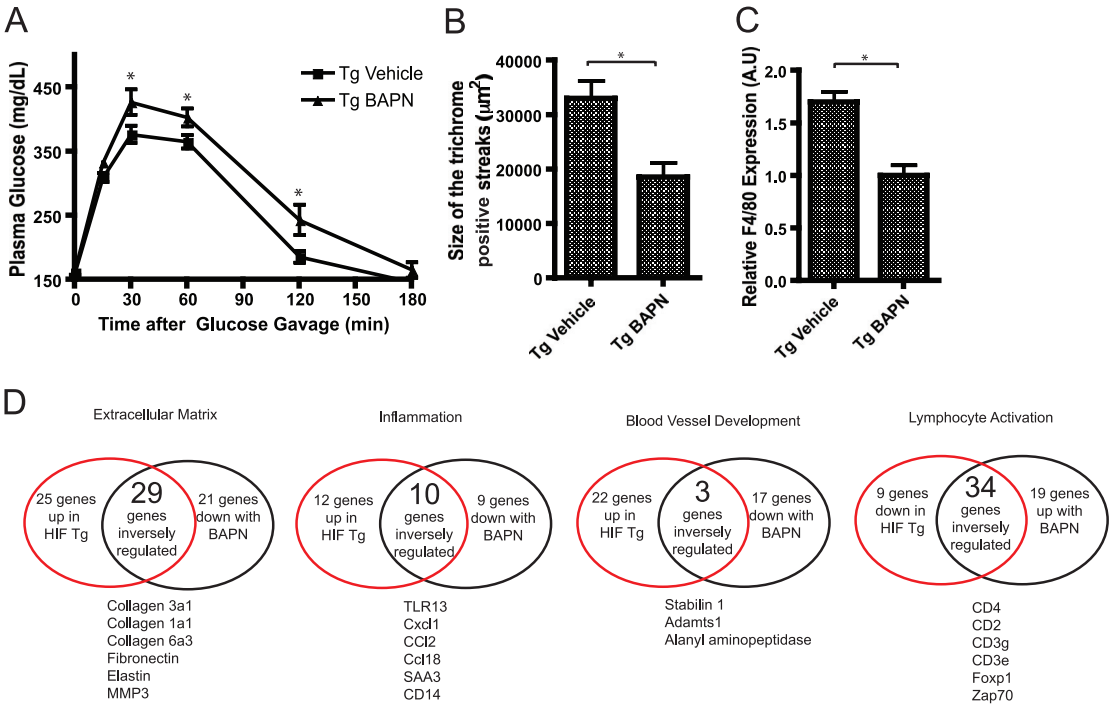

FIG. 6. Inhibition of LOX by BAPN treatment leads to an improved metabolic phenotype. (A) Circulating glucose during OGTT of HIF1α-ΔODD mice treated with either vehicle or the LOX inhibitor BAPN for the last 2 weeks of a 5-week HFD experiment (four mice/group). Tg, transgenic mice. (B) Quantification of the collagen-loaded streaks using ImageJ in the SWAT of HIF1α-ΔODD mice treated with either vehicle or the LOX inhibitor BAPN. Bar corresponds to 25 μm (four mice/group). (C) SWAT expression of F4/80 (Emr1) in HIF1α-ΔODD treated with either vehicle or the LOX inhibitor BAPN for the last 2 weeks of a 5-week HFD, as measured by quantitative RT-PCR (four mice/group). A.U, arbitrary units. (D) Schematic illustration of the inverse overlap between the microarray analysis of HIF transgenic versus wild-type mice, with HIF transgenic mice treated with either vehicle or the LOX inhibitor BAPN. Specifically, four important gene clusters are shown, as follows: extracellular matrix, inflammation, blood vessel development, and lymphocyte activation. Shown in the red circle is the number of genes changed by the HIF transgene compared to that of wild-type mice. The black circle, on the other hand, contains the number of genes that were altered by the LOX inhibitor BAPN in the HIF transgenic mice. Underneath each cluster are examples of inversely regulated genes. Panel A is analyzed by the two-way ANOVA for repeated measures; panels B and C are analyzed by Student's *t* test. *, $P < 0.05$.

HIF target (11) and that the HIF1α-ΔODD mice mediated an upregulation of LOX, we considered whether LOX might indeed function as a critical mediator of metabolic dysfunction triggered by HIF1α-ΔODD overexpression. As BAPN is a conventional inhibitor of LOX, we further decided to subject HIF1α-ΔODD mice to a 2-week BAPN treatment regimen. While BAPN had no significant effect on wild-type mice (data not shown), BAPN induced significant improvements at the level of whole-body glucose tolerance in HIF1α-ΔODD mice (Fig. 6A) while not causing any significant changes in body weight over the course of the treatment (data not shown). BAPN treatment was further shown to affect adipose tissue fibrosis locally, leading to a significant reduction of the size of the collagen-laden trichrome-stained streaks (Fig. 6B). Along with this reduction in fibrillar collagens, a reduction in macrophage infiltration was observed, as noted by a reduced level of F4/80 expression in transgenic mice treated with BAPN (Fig. 6C). To further gauge how important HIF1α-induced LOX expression is for the total effects of HIF1α in adipose tissue, we performed a microarray analysis of SWAT and EWAT of the transgenic mice treated with either BAPN or vehicle. This microarray analysis confirmed the reduction in proinflammatory markers (data not shown). More importantly, however, we were surprised to find that the expression of ~900 genes that were identified in the original HIF1α transgenic mice to be dysregulated was reversed upon BAPN treatment. Examining the most important gene clusters affected by HIF1α, we found a vast inverse overlap between the two microarrays. Figure 6G shows that 54% (29 out of 54 genes) of the genes upregulated by the HIFα transgene in the extracellular cluster are downregulated by BAPN in the HIF1α-ΔODD mice. These genes include several essential components of the extracellular matrix and fibrillar collagens, in particular. Some examples are Col1α1, Col3α1, Col6α3, elastin, lumican, and fibronectin. The same degree of overlap was found in the inflammation cluster (45%; 10 of 22 genes), whereas we did not see that with the angiogenesis cluster (12%; 3 of 25 genes). As with the general inflammatory pathway, the marked reductions in T-cell activation markers seen in the HIF1α-ΔODD mice are also largely dependent on HIF1α's ability to induce LOX (79%; 34 of 43 genes).

While we cannot rule out additional pathways critically affected by HIF1α action in adipocytes, these results clearly identify LOX as an important downstream contributor toward HIF1α-mediated metabolic dysregulation of adipose tissue.

Refined time course of an HFD. By characterizing the HIF1α-ΔODD mice, we have demonstrated that hypoxia-inducible HIF1α can cause fibrosis in adipose tissue, at least in

part, by induction of LOX. To further validate this mechanism, we chose to analyze the first 20 days after the initial exposure to an HFD at high temporal resolution. Based on the findings described above, we would predict that the acute increase in adipocyte size that follows an acute HFD turns on a gene program, including HIF and LOX. To get a more discrete separation of the metabolic events induced by the HFD, we decided to use C57/B6 mice from Charles River Laboratories (CRL). We found that the rate at which CRL C57/B6 mice develop HFD-induced glucose intolerance is significantly lower than mice with the same genetic background purchased from Jackson Laboratories (Z. V. Wang and P. E. Scherer, unpublished observations).

Body weights increased by 2 g within 2 days of the initiation of the HFD (Fig. 7A). The rate of weight gain on a chow diet is significantly lower at that age (not shown). This consequently resulted in almost a doubling of the adipocyte size (Fig. 7B). After 4 days, both body weight and adipocyte area keep increasing, although at a much lower rate. Interestingly, the immediate adipocyte cell expansion led to an increase in HIF1α message levels in the SWAT (Fig. 7C). This in turn leads to an even more pronounced increase in LOX expression (Fig. 7D). Whereas the HIF1α mRNA levels stay up over the 20 days, the LOX expression gets repressed by an unknown mechanism and decreases to pre-HFD levels after 10 days. Both collagen I and III follow a pattern very similar to that of LOX (Fig. 7E and F). These results are consistent with our proposed temporal sequence of events that are initiated by an early hypoxic response due to a massive expansion of adipocyte size, followed by an induction of ECM proteins. We furthermore suggest that these processes are culminating with the infiltration of macrophages only at later stages of the time course. Here, we were unable to detect an increase in the F4/80 message (as an indicator of macrophage infiltration), number of crown-like structures, and general upregulation of inflammatory markers such as tumor necrosis factor alpha (TNF-α) until 13 days postinitiation of HFD (Fig. 7G to I).

Respiratory hypoxia induces fibrotic genes in white adipose tissue. In a final set of experiments, we sought to confirm the observations described above in an independent setting. Does adipose tissue also react to other hypoxic challenges, such as chronically lowered oxygen levels in a hypoxia chamber, in a way similar to that during fat pad expansion? If so, would adipose tissue respond by turning on the same fibrotic gene expression pattern as those in obese and HIF1α transgenic mice? This was indeed the case. By exposing wild-type mice to 10% oxygen for 48 h and 5 days, the expression of LOX and collagen I and III all increased, whereas neither VEGFa nor F4/80 was significantly affected in SWAT and GLUT1 was only slightly upregulated (Fig. 8A and B). Whereas LOX expression was stable between 48 h and 5 days of hypoxia, both collagen I and III were expressed to even higher levels after 5 days of hypoxia. Since none of these collagens are established HIF targets, this points toward an alternative hypoxia-mediated regulation of the expression levels of these genes. The fact that *ob*/*ob* mice do not have markedly increased expression of the collagens is inconsistent with such an idea. We would anticipate that the respiratory hypoxia would result in a similar state of hypoxia in tissues, but interestingly, expression of LOX was decreased rather than increased in muscle, providing further evidence for a tissue-specific response to hypoxia (see Fig. S21 and S22 in the supplemental material).

DISCUSSION

Adipose tissue from obese individuals displays several prominent features not typically observed in the lean state; to accommodate an excessive triglyceride load, adipose tissue expands through both adipocyte hypertrophy and hyperplasia. This expansion is furthermore associated with hypoxia, fibrosis, local inflammation, and concomitant insulin resistance. While local inflammation and insulin resistance in adipose tissue are causally related to systemic metabolic dysfunction and type II diabetes, the temporal and mechanistic connections among the processes prior to inflammation have not, as yet, been characterized. Nevertheless, late-stage processes related to the interaction between adipose tissue inflammation and insulin sensitivity, however, are better understood. Several components of the inflammatory pathways have been implicated in reducing insulin sensitivity, such as TNF-α (21), c-jun N-terminal kinase (19), and NF-κB (54). The associated infiltration of monocytes and macrophages into adipose tissue has been extensively studied (50, 52). Whether such an infiltration is strictly secondary to concomitant necrosis of adipocytes during fat expansion or is the result of enhanced chemokine secretion by enlarged adipocytes, or is a combination of the two, remains unclear. From cell culture studies, we know that the three-dimensional network of the extracellular matrix surrounding the adipocyte is functionally very important (5, 43). We have recently demonstrated that fibrosis of the adipose tissue plays an important role in adipose tissue dysfunction (28). Here, we show that obese adipose tissue contains large streaks that stain positively for fibrillar collagens, interspersed in between adipocytes. In Khan et al. (28), we have furthermore demonstrated that the genetic removal of a key constituent of the adipose tissue extracellular matrix, collagen VI, leads to a significant improvement in the metabolic phenotype of mice challenged with a dietary intervention or in the *ob*/*ob* background. Reduced macrophage infiltration in these collagen VI null mice indicates a connection among alterations in the adipose tissue extracellular matrix, adipocyte survival, and inflammation. Here, we sought to identify the upstream mechanisms that trigger the accumulation of extracellular matrix components that ultimately lead to fibrosis. We found that local adipose tissue hypoxia may be the most important driving force for the downstream events associated with adipose tissue dysfunction.

As oxygen diffuses away from the capillary bed, its partial pressure falls from approximately 100 mmHg inside the vessel to almost zero within as little as 100 μm into the tissue (14). Considering adipocytes are rather large cells, with diameters of up to 200 μm (42), the hypoxic phenomenon is prone to be relevant based on the sheer size of the adipocyte. Additionally, obese adipose tissue displays an attenuated increase in postprandial blood flow (7, 45), which is in part due to reduced insulin sensitivity of the cells in the vessels (26, 48). Consequently, obesity-associated adipose tissue hypoxia has been demonstrated by several groups in human adipose tissue (3, 13, 24) and in rodent adipose tissue (20, 37, 53). These initial findings led to the hypothesis that local adipose tissue hypoxia

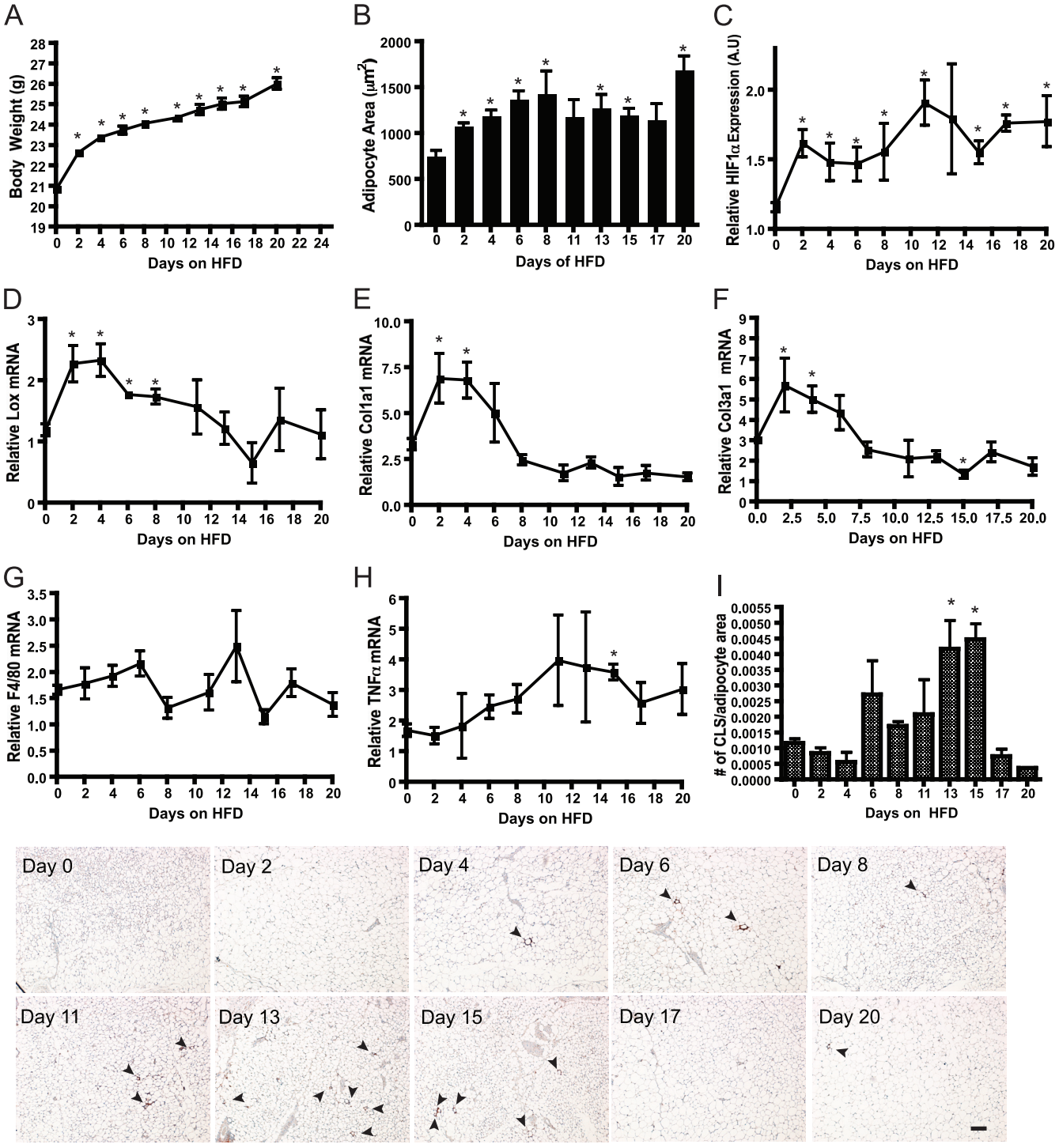

FIG. 7. Refined HFD time course. (A) Body weight of wild-type mice fed an HFD for 20 days. (B) Adipocyte area of the SWAT compartment during 20 days of an HFD in wild-type mice. (C to H) mRNA levels of HIF1α, LOX, Col1a1, Col3a1, F4/80, and TNF-α in the SWAT of wild-type mice fed an HFD for 20 days. A.U, arbitrary units. (I) Detection of crown-like structures (indicated by arrowheads) by immunoreactive MAC-2 in SWAT before and during 20 days of an HFD. (A to I) Three mice/time point. CLS, crownlike structure. Data were analyzed by the Student's *t* test. *, $P < 0.05$.

may underlie the inflammatory response (47); however, direct evidence for such a mechanism has been lacking to date.

Hypoxia in adipose tissue results in the stabilization of the transcription factor HIF1 (3, 49, 53). This master regulator of the hypoxia response has been thoroughly investigated in the context of tumor biology. Its major effect is the induction of an angiogenic response through binding to the hypoxia response element of target genes, such as VEGFa and angiopoietin 2.

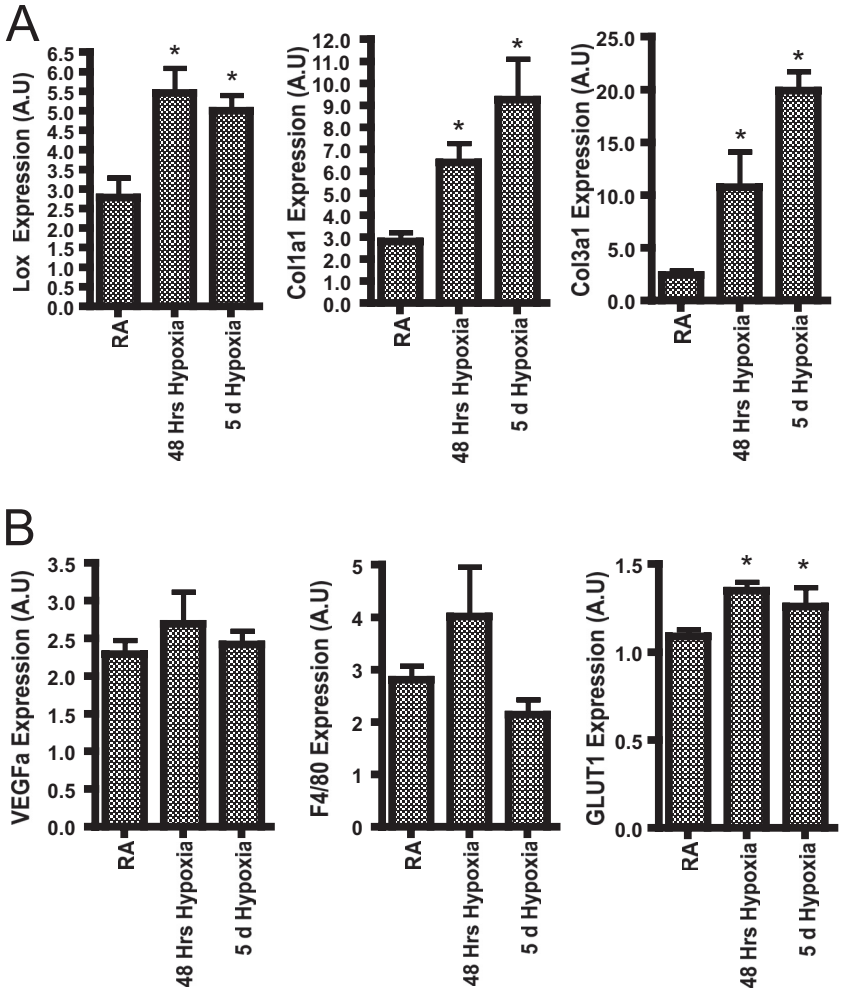

FIG. 8. Respiratory hypoxia. Expression levels of LOX, Col1a1, Col3a1, GLUT1, F4/80, and VEGFa in the SWAT (A) and muscle (B) in mice breathing ambient air or 10% O_2 for 48 h and 10% O_2 for 5 days, as measured by quantitative RT-PCR. All data were analyzed by Student's *t* test, with four mice/group. *, $P < 0.05$; A.U, arbitrary units.

This, in turn, allows the tumor to establish a better oxygenated and nutritionally-enriched microenvironment (1). Tumors can divert their pyruvate metabolism away from the mitochondrial electron transport chain toward an anaerobic conversion into lactate through a process that is largely mediated by HIF1α (40). Here, our objectives were to characterize the role of HIF1α in large adipocytes and to investigate any possible connections between HIF1α and fibrosis. In order to achieve that, we took advantage of the overexpression of a dominant active deletion mutant of HIF1α (HIF1α-ΔODD). With this transgene, we failed to detect any transcriptional increase in some of the classical HIF1α targets such as VEGF-A as well as failed to observe an accompanying increase in angiogenesis and anaerobic glycolysis. However, HIF1α-ΔODD overexpression did result in a transgene-dependent global glucose intolerance that could be enhanced by age, diet, and genetically induced obesity. Further profiling of the transgenic fat highlighted the critical transcriptional targets. Such targets included a general HIF1α-induced increase in fibrotic proteins such as LOX, elastin, collagen I and III, TIMP1, and CTGF. Induction of such a fibrotic program resulted in increased fibrillar collagen (I and III) accumulation in the extracellular matrix of the adipose tissue in the transgenic animals, thereby turning wild-type fat pads into tissue resembling fat from *ob*/*ob* mice. This is consistent with several cell culture studies that have previously demonstrated that hypoxia increases the expression of extracellular proteins, such as collagen I, fibronectin, and TIMP1, in various mesenchymal cell lines as well as in human renal fibroblasts (8, 12, 34). More importantly, however, to the production of collagens and other extracellular matrix constituents, the strength of this matrix is highly dependent on further processing of the components. One such enzyme that plays a critical role in the stabilization of the extracellular matrix components is LOX, which can cross-link elastins and collagens in the extracellular matrix and thus increase extracellular tensile strength. Since LOX is a known HIF1 target gene, we decided to investigate the functional role of LOX in rapidly expanding adipose tissue. The LOX gene is highly responsive to metabolic cues and is generally upregulated in situations characterized by dysfunctional adipose tissue such as obesity or exposure to endotoxin. On the other hand, PPARγ agonist treatment and adipogenesis are characterized by a significant reduction in

LOX gene expression. Within as little as 5 weeks of HFD exposure, prior to any weight differences between our transgenic HIF1α-ΔODD and wild-type mice, the transgenic mice displayed increased expression of LOX as well as a decrease in glucose tolerance and increased adipose tissue fibrosis. The increased fibrosis was even more pronounced as the HIF1α-ΔODD mice were genetically challenged by crossing them into the *ob*/*ob* background. Pharmacological inhibition of LOX activity resulted in an increase in the insulin sensitivity of HIF1α-overexpressing animals. Microarray analysis furthermore showed that approximately half the genes upregulated by HIF1α are dependent on HIF1α-induced LOX expression. As such, our studies pinpoint LOX as a key player in HIF1α-mediated fibrosis and associated insulin resistance. However, this does not rule out important contributions of other HIF1α targets. As such, another interesting candidate could be CTGF, which has been shown to be regulated in a fashion similar to that of LOX in the adipocyte (46). Like the findings presented here, Higgins et al. have demonstrated that renal hypoxia leads to a HIF1α-mediated fibrosis through induction of LOX (18). Interestingly, aside from its effects on collagens and elastins in the extracellular space, LOX has been detected inside the nuclear compartment of the cell as well (31), where it may function as a transcription factor for elastin and collagen III (15, 35). Nuclear LOX may further compound the effects of HIF1α on fibrosis in adipose tissue.

Throughout all experiments performed, we noticed that the effects we observed were strictly dependent on the local levels of expression of the transgene. We observe this phenomenon of differential transgene expression driven by the aP2 promoter in different fat pads quite frequently in several unrelated instances. This phenomenon is a function of the integration site of the transgene. While uniform transgene expression in different fat pads can be achieved with this promoter (resulting in more-severe systemic phenotypes), we decided to further characterize a transgenic line with differential expression levels in different fat pads, such that we can use fat pads with low transgene expression levels as internal controls for comparisons with fat pads with high transgene expression levels.

The induction of collagen I- and III-laden "trichrome-positive streaks" during the early stages of adipose tissue dysfunction is intriguing. Such structures are highly obvious when comparing adipose tissue from *ob*/*ob* animals to that of wild-type animals. They can, however, further be detected under conditions with much milder metabolic alterations associated with HIF1α overexpression in younger mice. Furthermore, these structures are distinct from the "crown-like structures" previously defined by Strissel and colleagues (44) and are apparent before these crown-like structures start to appear. It is technically very difficult to establish a direct relationship between trichrome-positive streaks and crown-like structures, but it is tempting to speculate that such "fibrotic streaks" reflect local hypoxic pockets that will ultimately be associated with increased necrosis of the surrounding adipocytes that will eventually attract macrophages to form crown-like structures. Our detailed time course analysis over the first 20 days of an HFD showed that the fibrotic program (e.g., HIF1α, LOX, collagen I and III) is induced shortly after initiation of the HFD challenge. Macrophages and the associated inflammation appear much later in the process.

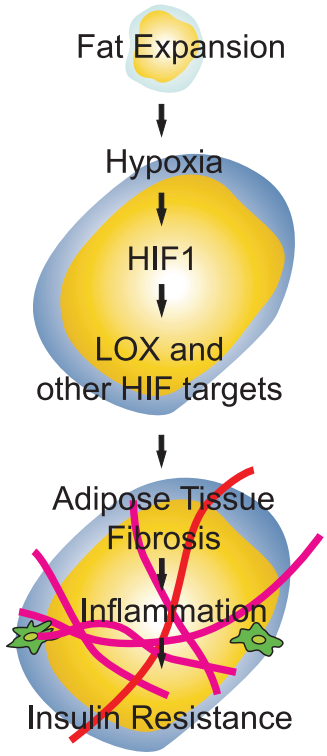

FIG. 9. Schematic representation of the suggested hypothesis. During periods of a positive-energy balance, white adipose tissue expands to meet the need for extra triglyceride storage. As a consequence, adipose tissue becomes hypoxic, thereby activating the transcription factor HIF1α. HIF1α in turn activates a host of genes involved in several physiological responses. Here, we demonstrate that this HIF1α activation initiates a fibrotic response and causes insulin resistance in white adipose tissue. Furthermore, we show that HIF1 induces the collagen cross-linker LOX, which plays a crucial part in this process. Finally, we hypothesize that HIF1-induced fibrosis can be the initiating factor for monocyte infiltration and inflammation.

It is unlikely that hypoxia affects an expanding fat pad uniformly but rather develops from pockets that are initially less vascularized. Additionally, it is by now well established that the epididymal fat pad in rodents expands asymmetrically, with the tip of this fat pad expanding most dramatically (4).

As evident by Fig. S3 in the supplemental material, the HIF1α transgene is expressed in brown adipose tissue as well as in white adipose tissue. However, we have not been able to detect any local phenotypic changes with respect to histology (H&E and trichrome staining), gene expression, or Western blotting in brown adipose tissue (data not shown). We therefore cannot draw any conclusions with respect to the function of HIF1α in brown adipose tissue and have consequently chosen to focus solely on white adipose tissue in the present study. However, this does not mean than HIF1α does not exert potentially important functions in brown adipose tissue. The lack of a phenotypic change in brown adipocytes is most likely a reflection of a low level of transgene expression in this particular fat pad.

In light of our data presented here, we would like to propose the following model for the early stages of adipose tissue dysfunction (Fig. 9): excess caloric intake results in an expansion

of adipose tissue. Such expansion causes local adipose tissue hypoxia, which triggers increased expression and stabilization of HIF1α. Despite its enhanced expression HIF1α fails to alleviate hypoxia, due to its inability to induce proangiogenic factors. However, HIF1α does stimulate a host of extracellular factors, such as collagens, in addition to components involved in establishing and remodeling the extracellular matrix. Most notably, LOX exerts a prominent role in this remodeling that leads to an increased deposition of fibrillar collagen in the adipose tissue. This global upregulation of extracellular matrix constituents subsequently causes fibrosis, and it is this fibrosis per se that results in increased stress of expanding adipocytes as well as necrosis. As a consequence, this triggers an increased infiltration of macrophages that ultimately mediates higher levels of local inflammation and a concomitant reduction in insulin sensitivity.

ACKNOWLEDGMENTS

We thank members of the Scherer laboratory for helpful discussions and assistance. We thank Ken Chen and the transgenic core facility at the Albert Einstein College of Medicine for transgenic mouse generation; Virginia Liu, Amy Song, and James Yi for technical assistance; the University of Texas Southwestern Metabolic Core for phenotyping efforts; and Joyce Repa for help with isolation of primary macrophages. Finally, we thank John Shelton and James Richardson in the Molecular Pathology Core at the University of Texas Southwestern for expert assistance with histology.

This work was supported by NIH grants R01-DK55758 and R01-CA112023 (P.E.S.) and by the TORS Consortium Grant (1PL1DK 081182). N.H. is supported by a stipend from the Faculty of Health Science of the University of Copenhagen.

REFERENCES

1. **Brahimi-Horn, M. C., J. Chiche, and J. Pouyssegur.** 2007. Hypoxia and cancer. J. Mol. Med. **85:**1301–1307.
2. **Brakenhielm, E., R. Cao, B. Gao, B. Angelin, B. Cannon, P. Parini, and Y. Cao.** 2004. Angiogenesis inhibitor, TNP-470, prevents diet-induced and genetic obesity in mice. Circ. Res. **94:**1579–1588.
3. **Cancello, R., C. Henegar, N. Viguerie, S. Taleb, C. Poitou, C. Rouault, M. Coupaye, V. Pelloux, D. Hugol, J. L. Bouillot, A. Bouloumie, G. Barbatelli, S. Cinti, P. A. Svensson, G. S. Barsh, J. D. Zucker, A. Basdevant, D. Langin, and K. Clement.** 2005. Reduction of macrophage infiltration and chemoattractant gene expression changes in white adipose tissue of morbidly obese subjects after surgery-induced weight loss. Diabetes **54:**2277–2286.
4. **Cho, C. H., Y. J. Koh, J. Han, H. K. Sung, H. Jong Lee, T. Morisada, R. A. Schwendener, R. A. Brekken, G. Kang, Y. Oike, T. S. Choi, T. Suda, O. J. Yoo, and G. Y. Koh.** 2007. Angiogenic role of LYVE-1-positive macrophages in adipose tissue. Circ. Res. **100:**e47–e57.
5. **Chun, T. H., K. B. Hotary, F. Sabeh, A. R. Saltiel, E. D. Allen, and S. J. Weiss.** 2006. A pericellular collagenase directs the 3-dimensional development of white adipose tissue. Cell **125:**577–591.
6. **Combs, T. P., U. B. Pajvani, A. H. Berg, Y. Lin, L. A. Jelicks, M. Laplante, A. R. Nawrocki, M. W. Rajala, A. F. Parlow, L. Cheeseboro, Y. Y. Ding, R. G. Russell, D. Lindemann, A. Hartley, G. R. Baker, S. Obici, Y. Deshaies, M. Ludgate, L. Rossetti, and P. E. Scherer.** 2004. A transgenic mouse with a deletion in the collagenous domain of adiponectin displays elevated circulating adiponectin and improved insulin sensitivity. Endocrinology **145:**367–383.
7. **Coppack, S. W., R. M. Fisher, G. F. Gibbons, S. M. Humphreys, M. J. McDonough, J. L. Potts, and K. N. Frayn.** 1990. Postprandial substrate deposition in human forearm and adipose tissues in vivo. Clin. Sci. (London) **79:**339–348.
8. **Distler, J. H., A. Jungel, M. Pileckyte, J. Zwerina, B. A. Michel, R. E. Gay, O. Kowal-Bielecka, M. Matucci-Cerinic, G. Schett, H. H. Marti, S. Gay, and O. Distler.** 2007. Hypoxia-induced increase in the production of extracellular matrix proteins in systemic sclerosis. Arthritis Rheum. **56:**4203–4215.
9. **Edelson, P. J., R. Zwiebel, and Z. A. Cohn.** 1975. The pinocytic rate of activated macrophages. J. Exp. Med. **142:**1150–1164.
10. **Elson, D. A., G. Thurston, L. E. Huang, D. G. Ginzinger, D. M. McDonald, R. S. Johnson, and J. M. Arbeit.** 2001. Induction of hypervascularity without leakage or inflammation in transgenic mice overexpressing hypoxia-inducible factor-1alpha. Genes Dev. **15:**2520–2532.
11. **Erler, J. T., K. L. Bennewith, M. Nicolau, N. Dornhofer, C. Kong, Q. T. Le, J. T. Chi, S. S. Jeffrey, and A. J. Giaccia.** 2006. Lysyl oxidase is essential for hypoxia-induced metastasis. Nature **440:**1222–1226.
12. **Falanga, V., T. A. Martin, H. Takagi, R. S. Kirsner, T. Helfman, J. Pardes, and M. S. Ochoa.** 1993. Low oxygen tension increases mRNA levels of alpha 1 (I) procollagen in human dermal fibroblasts. J. Cell. Physiol. **157:**408–412.
13. **Fleischmann, E., A. Kurz, M. Niedermayr, K. Schebesta, O. Kimberger, D. I. Sessler, B. Kabon, and G. Prager.** 2005. Tissue oxygenation in obese and non-obese patients during laparoscopy. Obes. Surg. **15:**813–819.
14. **Folkman, J., P. Hahnfeldt, and L. Hlatky.** 2000. Cancer: looking outside the genome. Nat. Rev. Mol. Cell Biol. **1:**76–79.
15. **Giampuzzi, M., G. Botti, M. Di Duca, L. Arata, G. Ghiggeri, R. Gusmano, R. Ravazzolo, and A. Di Donato.** 2000. Lysyl oxidase activates the transcription activity of human collagene III promoter. Possible involvement of Ku antigen. J. Biol. Chem. **275:**36341–36349.
16. **Guy, C. T., R. D. Cardiff, and W. J. Muller.** 1992. Induction of mammary tumors by expression of polyomavirus middle T oncogene: a transgenic mouse model for metastatic disease. Mol. Cell. Biol. **12:**954–961.
17. **Higgins, D. F., M. P. Biju, Y. Akai, A. Wutz, R. S. Johnson, and V. H. Haase.** 2004. Hypoxic induction of Ctgf is directly mediated by Hif-1. Am. J. Physiol. Renal Physiol. **287:**F1223–F1232.
18. **Higgins, D. F., K. Kimura, W. M. Bernhardt, N. Shrimanker, Y. Akai, B. Hohenstein, Y. Saito, R. S. Johnson, M. Kretzler, C. D. Cohen, K. U. Eckardt, M. Iwano, and V. H. Haase.** 2007. Hypoxia promotes fibrogenesis in vivo via HIF-1 stimulation of epithelial-to-mesenchymal transition. J. Clin. Investig. **117:**3810–3820.
19. **Hirosumi, J., G. Tuncman, L. Chang, C. Z. Gorgun, K. T. Uysal, K. Maeda, M. Karin, and G. S. Hotamisligil.** 2002. A central role for JNK in obesity and insulin resistance. Nature **420:**333–336.
20. **Hosogai, N., A. Fukuhara, K. Oshima, Y. Miyata, S. Tanaka, K. Segawa, S. Furukawa, Y. Tochino, R. Komuro, M. Matsuda, and I. Shimomura.** 2007. Adipose tissue hypoxia in obesity and its impact on adipocytokine dysregulation. Diabetes **56:**901–911.
21. **Hotamisligil, G. S., N. S. Shargill, and B. M. Spiegelman.** 1993. Adipose expression of tumor necrosis factor-alpha: direct role in obesity-linked insulin resistance. Science **259:**87–91.
22. **Hu, C. J., A. Sataur, L. Wang, H. Chen, and M. C. Simon.** 2007. The N-terminal transactivation domain confers target gene specificity of hypoxia-inducible factors HIF-1alpha and HIF-2alpha. Mol. Biol. Cell **18:**4528–4542.
23. **Huang, L. E., J. Gu, M. Schau, and H. F. Bunn.** 1998. Regulation of hypoxia-inducible factor 1alpha is mediated by an O2-dependent degradation domain via the ubiquitin-proteasome pathway. Proc. Natl. Acad. Sci. USA **95:**7987–7992.
24. **Kabon, B., A. Nagele, D. Reddy, C. Eagon, J. W. Fleshman, D. I. Sessler, and A. Kurz.** 2004. Obesity decreases perioperative tissue oxygenation. Anesthesiology **100:**274–280.
25. **Kagan, H. M., and W. Li.** 2003. Lysyl oxidase: properties, specificity, and biological roles inside and outside of the cell. J. Cell. Biochem. **88:**660–672.
26. **Karpe, F., B. A. Fielding, V. Ilic, I. A. Macdonald, L. K. Summers, and K. N. Frayn.** 2002. Impaired postprandial adipose tissue blood flow response is related to aspects of insulin sensitivity. Diabetes **51:**2467–2473.
27. **Keller, M. P., Y. Choi, P. Wang, D. Belt Davis, M. E. Rabaglia, A. T. Oler, D. S. Stapleton, C. Argmann, K. L. Schueler, S. Edwards, H. A. Steinberg, E. Chaibub Neto, R. Kleinhanz, S. Turner, M. K. Hellerstein, E. E. Schadt, B. S. Yandell, C. Kendziorski, and A. D. Attie.** 2008. A gene expression network model of type 2 diabetes links cell cycle regulation in islets with diabetes susceptibility. Genome Res. **18:**706–716.
28. **Khan, T., E. S. Muise, P. Iyengar, Z. V. Wang, M. Chandalia, N. Abate, B. B. Zhang, P. Bonaldo, S. Chua, and P. E. Scherer.** 2009. Metabolic dysregulation and adipose tissue fibrosis: role of collagen VI. Mol. Cell. Biol. **29:**1575–1591.
29. **Kim, J. Y., E. van de Wall, M. Laplante, A. Azzara, M. E. Trujillo, S. M. Hofmann, T. Schraw, J. L. Durand, H. Li, G. Li, L. A. Jelicks, M. F. Mehler, D. Y. Hui, Y. Deshaies, G. I. Shulman, G. J. Schwartz, and P. E. Scherer.** 2007. Obesity-associated improvements in metabolic profile through expansion of adipose tissue. J. Clin. Investig. **117:**2621–2637.
30. **Kolonin, M. G., P. K. Saha, L. Chan, R. Pasqualini, and W. Arap.** 2004. Reversal of obesity by targeted ablation of adipose tissue. Nat. Med. **10:**625–632.
31. **Li, W., K. Nellaiappan, T. Strassmaier, L. Graham, K. M. Thomas, and H. M. Kagan.** 1997. Localization and activity of lysyl oxidase within nuclei of fibrogenic cells. Proc. Natl. Acad. Sci. USA **94:**12817–12822.
32. **Livak, K. J., and T. D. Schmittgen.** 2001. Analysis of relative gene expression data using real-time quantitative PCR and the 2(-delta delta C(T)) method. Methods **25:**402–408.
33. **Napolitano, L.** 1963. The differentiation of white adipose cells. An electron microscope study. J. Cell Biol. **18:**663–679.
34. **Norman, J. T., I. M. Clark, and P. L. Garcia.** 2000. Hypoxia promotes fibrogenesis in human renal fibroblasts. Kidney Int. **58:**2351–2366.
35. **Oleggini, R., N. Gastaldo, and A. Di Donato.** 2007. Regulation of elastin promoter by lysyl oxidase and growth factors: cross control of lysyl oxidase on TGF-beta1 effects. Matrix Biol. **26:**494–505.
36. **Pajvani, U. B., M. E. Trujillo, T. P. Combs, P. Iyengar, L. Jelicks, K. A. Roth, R. N. Kitsis, and P. E. Scherer.** 2005. Fat apoptosis through targeted activation of caspase 8: a new mouse model of inducible and reversible lipoatrophy. Nat. Med. **11:**797–803.

37. **Rausch, M. E., S. Weisberg, P. Vardhana, and D. V. Tortoriello.** 2008. Obesity in C57BL/6J mice is characterized by adipose tissue hypoxia and cytotoxic T-cell infiltration. Int. J. Obes. (London) **32:**451–463.
38. **Rupnick, M. A., D. Panigrahy, C. Y. Zhang, S. M. Dallabrida, B. B. Lowell, R. Langer, and M. J. Folkman.** 2002. Adipose tissue mass can be regulated through the vasculature. Proc. Natl. Acad. Sci. USA **99:**10730–10735.
39. **Semenza, G. L.** 2007. Evaluation of HIF-1 inhibitors as anticancer agents. Drug Discov. Today **12:**853–859.
40. **Semenza, G. L.** 2007. Life with oxygen. Science **318:**62–64.
41. **Semenza, G. L.** 2003. Targeting HIF-1 for cancer therapy. Nat. Rev. Cancer **3:**721–732.
42. **Skurk, T., C. Alberti-Huber, C. Herder, and H. Hauner.** 2007. Relationship between adipocyte size and adipokine expression and secretion. J. Clin. Endocrinol. Metab. **92:**1023–1033.
43. **Spiegelman, B. M., and C. A. Ginty.** 1983. Fibronectin modulation of cell shape and lipogenic gene expression in 3t3-adipocytes. Cell **35:**657–666.
44. **Strissel, K. J., Z. Stancheva, H. Miyoshi, J. W. Perfield II, J. DeFuria, Z. Jick, A. S. Greenberg, and M. S. Obin.** 2007. Adipocyte death, adipose tissue remodeling, and obesity complications. Diabetes **56:**2910–2918.
45. **Summers, L. K., J. S. Samra, S. M. Humphreys, R. J. Morris, and K. N. Frayn.** 1996. Subcutaneous abdominal adipose tissue blood flow: variation within and between subjects and relationship to obesity. Clin. Sci. (London) **91:**679–683.
46. **Tan, J. T., S. V. McLennan, W. W. Song, L. W. Lo, J. G. Bonner, P. F. Williams, and S. M. Twigg.** 2008. Connective tissue growth factor inhibits adipocyte differentiation. Am. J. Physiol. Cell Physiol. **295:**C740–C751.
47. **Trayhurn, P., and I. S. Wood.** 2004. Adipokines: inflammation and the pleiotropic role of white adipose tissue. Br. J. Nutr. **92:**347–355.
48. **Virtanen, K. A., P. Lonnroth, R. Parkkola, P. Peltoniemi, M. Asola, T. Viljanen, T. Tolvanen, J. Knuuti, T. Ronnemaa, R. Huupponen, and P. Nuutila.** 2002. Glucose uptake and perfusion in subcutaneous and visceral adipose tissue during insulin stimulation in nonobese and obese humans. J. Clin. Endocrinol. Metab. **87:**3902–3910.
49. **Wang, B., I. S. Wood, and P. Trayhurn.** 2007. Dysregulation of the expression and secretion of inflammation-related adipokines by hypoxia in human adipocytes. Pflugers Arch. **455:**479–492.
50. **Weisberg, S. P., D. McCann, M. Desai, M. Rosenbaum, R. L. Leibel, and A. W. Ferrante, Jr.** 2003. Obesity is associated with macrophage accumulation in adipose tissue. J. Clin. Investig. **112:**1796–1808.
51. **Woessner, J. F., Jr.** 1961. The determination of hydroxyproline in tissue and protein samples containing small proportions of this imino acid. Arch. Biochem. Biophys. **93:**440–447.
52. **Xu, H., G. T. Barnes, Q. Yang, G. Tan, D. Yang, C. J. Chou, J. Sole, A. Nichols, J. S. Ross, L. A. Tartaglia, and H. Chen.** 2003. Chronic inflammation in fat plays a crucial role in the development of obesity-related insulin resistance. J. Clin. Investig. **112:**1821–1830.
53. **Ye, J., Z. Gao, J. Yin, and Q. He.** 2007. Hypoxia is a potential risk factor for chronic inflammation and adiponectin reduction in adipose tissue of ob/ob and dietary obese mice. Am. J. Physiol. Endocrinol. Metab. **293:**E1118–E1128.
54. **Yuan, M., N. Konstantopoulos, J. Lee, L. Hansen, Z. W. Li, M. Karin, and S. E. Shoelson.** 2001. Reversal of obesity- and diet-induced insulin resistance with salicylates or targeted disruption of Ikkbeta. Science **293:**1673–1677.